Title
FLUID AND HEAT FLOW IN GAS-RICH GEOTHERMAL RESERVOIRS

Author
O'Sullivan, M.J.

Publication Date
1983-07-01

Lawrence Berkeley Laboratory
UNIVERSITY OF CALIFORNIA

EARTH SCIENCES DIVISION

To be presented at the Society of Petroleum Engineers Annual Technical Conference and Exhibition, San Francisco, CA, October 5-8, 1983

FLUID AND HEAT FLOW IN GAS-RICH GEOTHERMAL RESERVOIRS

M.J. O'Sullivan, G.S. Bodvarsson, K. Pruess, and M.R. Blakeley

July 1983

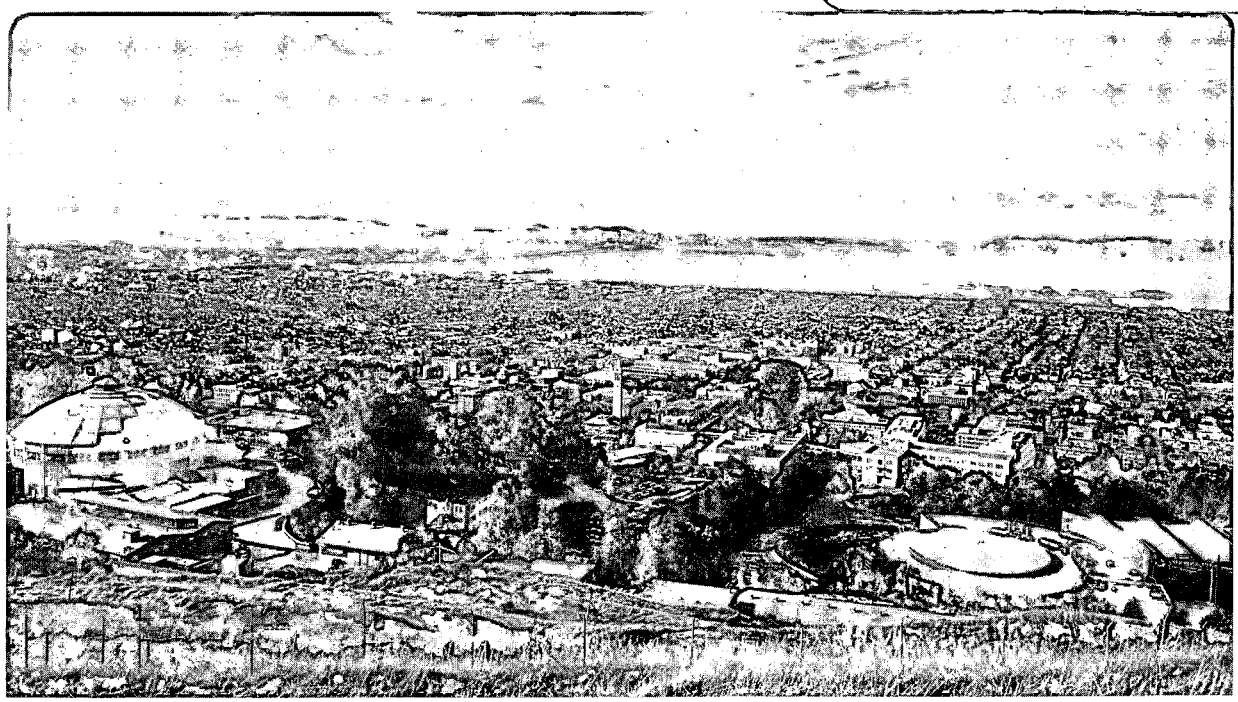

Prepared for the U.S. Department of Energy under Contract DE-AC03-76SF00098

DISCLAIMER

To be presented at the Society of Petroleum Engineers Annual Technical Conference and Exhibition, San Francisco, California, October 5-8, 1983

LBL-16329

Fluid and Heat Flow in Gas-Rich Geothermal Reservoirs

M. J. O'Sullivan[1], G. S. Bodvarsson, K. Pruess, and M. R. Blakeley[2]

Earth Sciences Division
Lawrence Berkeley Laboratory
University of California
Berkeley, California 94720

July 1983

[1] Permanent address: University of Auckland, New Zealand

[2] University of Auckland, New Zealand

This work was supported by the Assistant Secretary for Conservation and Renewable Energy, Office of Renewable Technology, Division of Geothermal and Hydropower Technologies of the U. S. Department of Energy under Contract No. DE-AC03-76SF00098

ABSTRACT

Numerical simulation techniques are used to study the effects of noncondensible gases (CO_2) on geothermal reservoir behavior in the natural state and during exploitation. It is shown that the presence of CO_2 has large effects on the thermodynamic conditions of a reservoir in the natural state, especially on temperature distributions and phase compositions. The gas will expand two-phase zones and increase gas saturations to enable flow of CO_2 through the system. During exploitation, the early pressure drop is primarily due to "degassing" of the system. This process can cause a very rapid initial pressure drop, on the order of tens of bars, depending upon the initial partial pressure of CO_2. The flowing gas content from wells can provide information on in-place gas saturations and relative permeability curves that apply at a given geothermal resource. Site-specific studies are made for the gas-rich two-phase reservoir at the Ohaaki geothermal field in New Zealand. A simple lumped-parameter model and a vertical column model are applied to the field data. The results obtained agree well with the natural thermodynamic state of the Ohaaki field (pressure and temperature profiles) and a partial pressure of 15-25 bars is calculated in the primary reservoirs. The models also agree reasonably well with field data obtained during exploitation of the field. The treatment of thermophysical properties of H_2O-CO_2 mixtures for different phase compositions is summarized.

INTRODUCTION

Many geothermal reservoirs contain large amounts of noncondensible gases, particularly carbon dioxide. The proportion of noncondensible gas in the produced fluid is an extremely important factor in the design of separators, turbines, heat exchangers, and other surface equipment. In the reservoir itself, the presence of carbon dioxide significantly alters the distribution of temperature and gas saturation (volumetric fraction of gas phase) associated with given heat and mass flows. Therefore, when modeling gas-rich reservoirs it is essential to keep track of the amount of CO_2 in each grid block in addition to the customary fluid and heat content.

The simulations reported in this paper were carried out using the multicomponent, two-phase, reservoir simulator MULKOM,[1] developed at Lawrence Berkeley Laboratory as an extension of the geothermal reservoir simulator SHAFT79.[2] MULKOM is coded in a general way to model the transport of energy and mass, with a separate mass balance equation for each component. All that is required for modeling the transport of a particular component such as carbon dioxide, is the addition of the appropriate thermodynamic "package", so that densities, viscosities, enthalpies, and other relevant thermophysical quantities can be calculated from the primary variables (e.g., pressure, temperature, and chemical composition). The H_2O-CO_2 thermodynamic package used in the present study is an improved version of the one used earlier by Zyvoloski and O'Sullivan[3] in a geothermal simulator developed at the University of Auckland. It is based mainly on work by Sutton and McNabb[4] on the properties of a mixture of carbon dioxide and water. A similar thermodynamic package was used by Pritchett, Rice, and Riney[5] together with their CHARGR simulator in a preliminary study on the effects of CO_2 in geothermal reservoirs.

Several investigators have considered the effects of CO_2 on the reservoir dynamics of geothermal systems. A lumped-parameter model using one block for the gas zone and one for the liquid zone was developed by Atkinson et al.[6] for the Bagnore (Italy) reservoir. Preliminary work on the Ohaaki reservoir was carried out by Zyvoloski and O'Sullivan[3,7,8], but these studies were limited because the thermodynamic package used could only handle two-phase conditions. Generic studies of reservoir depletion[5] and well-test analysis[3,5] were also made in the previous works. The present study describes the effects of CO_2 in geothermal reservoirs in a more complete and detailed way. We emphasize the potential for using the CO_2 content in the fluid produced during a well test as a reservoir diagnostic aid, and as a means of gaining information about relative permeability curves.

References and illustrations at end of paper.

The aim of the present study is to investigate the effects of CO_2 on both the natural state of a reservoir and its behavior under exploitation. Several generic simulation studies are described. First, the effect of CO_2 on the depletion of a single block, lumped-parameter reservoir model is briefly examined. Secondly, the relationship between the mass fraction of CO_2 in the produced fluid and the mass fraction in-place in the reservoir is studied. It is demonstrated that in some the relative permeability curves. Finally, the effects of CO_2 on the vertical distribution of gas saturation, temperature, and pressure of geothermal reservoirs in the natural state are investigated. The numerical simulator with the H_2O-CO_2 thermodynamic package is applied to field data from the Ohaaki (formerly Broadlands) geothermal field in New Zealand.

Two simple models of the 1966-1974 large-scale field exploitation test of the Ohaaki reservoir are presented. The first is a single-block, lumped-parameter model similar to those reported earlier by Zyvoloski and O'Sullivan[7], and Grant[9]. In the former work, a less accurate thermodynamic package for H_2O-CO_2 mixtures was used; the latter used approximate methods to integrate the mass-, energy-, and CO_2-balance equations. The second model described in the present work is a distributed-parameter model, in the form of a vertical column representing the main upflow zone at Ohaaki. This model produces a good fit to the observed distribution of pressure and temperature with depth[10] in the natural state at Ohaaki and a good match to the observed response of the reservoir during five years of experimental production and three years of recovery.

BASIC PROPERTIES OF CO_2-H_2O MIXTURES

A description of the H_2O-CO_2 thermodynamic package is given in the appendix, but some general results for the most important aspects of the behavior of a CO_2-H_2O mixture are discussed here.

In Figure 1, the mass fractions of CO_2 in the liquid phase and gas phase, respectively, of a boiling CO_2-H_2O mixture are shown as functions of temperature (the partial pressure of CO_2 is 10 bars). The figure shows that even for this moderately high partial pressure of CO_2, the total amount of CO_2 which can be dissolved in the liquid phase is small. Therefore, if a sufficiently large amount of CO_2 is introduced into a body of liquid water at fixed temperature and total pressure, the mixture must boil and evolve a gas phase. The gas phase contains a mixture of the excess CO_2 not dissolvable in the liquid, and water vapor at a partial pressure corresponding to the system temperature. For conditions of interest in geothermal systems, the mass of CO_2 present in a unit volume of gas phase is larger than that present in a unit volume of liquid phase. Therefore, if CO_2 partial pressure is kept constant, an increase in CO_2 mass fraction can only be accommodated by an increase in gas-phase saturation. A typical case is shown in Figure 2. We assume that a constant partial pressure of CO_2 (10 bars) and constant temperatures of 200°, 250°, or 300°C are maintained while the CO_2 mass fraction is increased. For the 250°C curve the CO_2 causes the mixture to boil as soon as it reaches a proportion of 0.49% by mass and then, as more and more CO_2 is added, the gas saturation increases until the liquid phase completely dissappears when the mass fraction of CO_2 reaches 33.5%. The increase of gas saturation which accompanies an increase in the mass fraction of CO_2 is the single most important effect of the CO_2, as the total mixture mobility greatly depends upon the volumetric fractions of liquid and gaseous phases present. The changes in density, viscosity, and enthalpy of the individual phases caused by the presence of CO_2 are comparatively minor.

The large difference in the mass fractions of CO_2 in liquid and gaseous phases is very important when calculating the mass fraction of CO_2 in two-phase fluids produced from a well, or flowing within the reservoir. The flowing enthalpy H_f is given by the well-known formula

$$H_f = \nu_f(H_\ell k_{r\ell}/\nu_\ell + H_g k_{rg}/\nu_g) \qquad (1)$$

where the total or flowing kinematic viscosity is defined by

$$1/\nu_f = k_{r\ell}/\nu_\ell + k_{rg}/\nu_g. \qquad (2)$$

A similar formula holds for the flowing CO_2 mass fraction f_{cf}:

$$f_{cf} = \nu_f(f_{c\ell} k_{r\ell}/\nu_\ell + f_{cg} k_{rg}/\nu_g) \qquad (3)$$

In (1), (2), and (3) the variation of the liquid and gas phase enthalpies, H_ℓ and H_g, and the kinematic viscosities of liquid and gas, ν_ℓ and ν_g, with total pressure, p, and partial pressure of CO_2, p_c, is relatively insignificant. The mass fractions of CO_2 in liquid and gas, $f_{c\ell}$ and f_{cg} vary with the partial pressure of CO_2. The relative permeabilities $k_{r\ell}$ and k_{rg} vary rapidly with changes in gas saturation S_g[11,12,13]. If the total pressure and temperature are fixed and the total mass fraction of CO_2 is increased so that the gas saturation increases (Fig. 2), then both the corresponding flowing enthalpy and flowing CO_2 mass fraction increase. How much they increase for a specified saturation change depends on the choice of the relative permeability curves. A simple algebraic calculation can be used to eliminate $k_{r\ell}$ and k_{rg} from (1), (2), and (3), giving the relationship

$$H_f = [f_{cf}(H_g - H_\ell) + (H_\ell f_{cg} - H_g f_{c\ell})]/(f_{cg} - f_{c\ell}) \qquad (4)$$

Equation (4) shows that, for fixed values of p and p_c, there is a simple linear relationship between flowing enthalpy and flowing CO_2 content. This relationship is shown in Figure 3 as solid lines for a temperature of 260°C and various values of the partial pressure of CO_2. The exact position on these curves for values obtained from production data from a particular well depends both on the gas saturation of the boiling mixture and on the relative permeability curves which apply. Also shown in Figure 3 are data points representing monthly samples taken from several wells at Ohaaki.[14] The temperature at the feed zone for the different wells varies but the corresponding curves are not

very different from those given in Figure 3. These points show production data after some initial degassing near the well has occurred and therefore are not inconsistent with estimates for the partial pressure in the main reservoir at Ohaaki[15], of up to 30 bar (see Figure 6).

To demonstrate the effect of CO_2 in a geothermal reservoir in a very simple way, the depletion of a lumped-parameter reservoir model was simulated. A block of volume 1.0 m^3 with porosity 0.15, density 2500 kg/m^3, and specific heat 900 J/kg°C, initially at a temperature of 260°C, a gas saturation of 0.2, and CO_2 partial pressures of either 0 or 30 bar was produced at a constant rate of 5 kg/s. The pressure decline curves for two sets of relative permeability curves, the Corey curves[16] and the Sorey, Grant, and Bradford[17] (SGB) curves (see Fig. 4) are shown in Figure 5. The small size of the block and the short time of simulation do not affect the applicability of the results for real geothermal reservoirs. The shape of the curves in Figure 5 would remain unchanged if both the volume and time scale were multiplied by the same factor. The most obvious feature of the decline curves is that the pressure drop due to "degassing" occurs rapidly. The flowing CO_2 mass fraction given by equation (3) is much greater than the mixture or in-place CO_2 mass fraction for gas saturations of 0.1 or greater, so that the CO_2 is quickly exhausted. The degassing period is considerably shorter for the SGB curves than for the Corey curves because of their greater gas mobility (see Fig. 4). The flowing enthalpy is decreased a small amount by the presence of CO_2 and therefore not as much heat is removed from the reservoir during the degassing period as for the $p_c = 0$ case. Consequently, for the cases with $p_c = 30$, the pressure remains slightly above that for $p_c = 0$. Also the density of the gassy fluid is slightly greater at T = 260°C and $S_g = 0.2$ than for pure boiling water and therefore the final depletion of the reservoir occurs sightly later. The qualitative nature of the results shown in Figure 5 also applies for other initial states.

CO_2 CONTENT IN PRODUCED FLUIDS

The relationship between flowing enthalpy and flowing CO_2 content given in (4) is not very useful in analyzing production data. For a constant-rate production test, assuming that the reservoir is uniform and infinite-acting, it can be shown[13,17,18] that the production enthalpy initially increases with time and eventually stabilizes at a constant value. The magnitude of the enthalpy rise depends in a complex manner on the initial state of the reservoir as well as on the porosity, relative permeabilities, and flow rate[13,17]. A calculation, similar to that carried out by O'Sullivan[18] using asymptotic methods to show that production enthalpy must stabilize, can also be used to show that the CO_2 content in the produced fluids must stabilize. Grant[19] gave an approximate derivation of this result for the special case of gas-dominated reservoirs.

A number of well-test simulations were carried out to investigate the relationship between production enthalpy and production CO_2 content. To make the results comparable to extensive field data from Ohaaki, New Zealand,[9,10,14] an initial temperature of 260°C was used and a number of different initial gas saturations and flow rates were tested. Reservoir response for different flow rates, permeabilities, and reservoir thicknesses depends only on the parameter group Q/kh; therefore the flow rate Q was varied but the permeability, k, and the reservoir thickness, h, were assumed constant. Figure 6 shows the results of some of these simulations. The solid curves show the loci of late-time stable production enthalpies, $H_f(\infty)$, and stable CO_2 mass fraction $f_{cf}(\infty)$, in dependence upon initial partial pressure of CO_2 and initial gas saturation, for a constant and relatively high flow rate. The general effect of flow rate is shown by the dotted and dashed curves which indicate the change in location of the solid curve network as flow rate is reduced. For example, for an initial CO_2 partial pressure of $p_{co} = 5$ bar and an initial gas saturation of $S_{go} = 0.3$, $H_f(\infty)$ and $f_{cf}(\infty)$ at the high flow rate are 1680 kJ/kg and 2.8%, respectively; at a very low flow rate they are 1293 kJ/kg and 2.3%, respectively.

All the results shown in Figure 6 were obtained using the Corey relative permeability curves. To show the effect of different relative permeabilities, some of the simulations were repeated using the SGB curves. The results are shown in Figure 7 (all for a high flow rate of 0.2 kg/s.m). The higher gas relative permeability recommended by Sorey et al[17] produces higher stable production enthalpies and even higher stable flowing CO_2 mass fractions. The effect of the different relative permeability curves is to extend the net so that lower initial gas saturations are required to produce similar enthalpies or CO_2 mass fractions. The effect of a different porosity is shown in Figure 8. The stable flowing enthalpy depends strongly on the ratio[13] $(1 - \phi)/\phi$, but the stable flowing CO_2 mass fraction is only weakly affected by porosity. Consequently, a change in porosity only shifts the curves along the vertical (enthalpy) axis.

DETERMINATION OF GAS SATURATION AND RELATIVE PERMEABILITIES

The results presented above show how variations in initial in-place conditions affect the production enthalpy and CO_2 mass fraction. In practice it is usually the inverse problem which is the important one. Namely: Given the production data what can be deduced about the thermodynamic state of the reservoir? It turns out that measurement of flowing CO_2 mass fraction can assist in determining in-place conditions. Bodvarsson et al.[13] showed how measurement of flowing enthalpy during a well test and equations (1) and (2) could be used to deduce the ratio $k_{rg}/k_{r\ell}$ as a function of flowing enthalpy. It was pointed out, however, that this procedure did not give k_{rg} and $k_{r\ell}$ individually, or their ratio as a function of gas saturation. Similarly, equations (2) and (3) could be used to deduce the ratio of $k_{rg}/k_{r\ell}$ as a function of flowing CO_2 mass fraction.

What is really required is a means of deducing gas saturation, or equivalently in-place enthalpy or in-place CO_2 mass fraction. A careful examination of Figures 6 and 8 indicate that it may be possible to deduce in-place gas saturation from the stable

flowing CO_2 mass fraction, $f_{cf}(\infty)$. The key points to observe are that $f_{cf}(\infty)$ depends very weakly on both flow rate and porosity, but strongly on initial saturation. Figure 9 shows the dependence of $f_{cf}(\infty)$ on saturation at various partial pressures. In Figure 9, the porosity was fixed at 0.1, the flow rate at 0.1 kg/s.m, and either the Corey or SGB relative permeability curves were used. Varying the porosity over the interval (0.05, 0.20), changes the curves in Figure 9 only slightly. This fact is demonstrated by the data shown in Table 1 where the stable flowing CO_2 mass fraction is tabulated for different porosities, and for some representative initial saturations. Similarly, Figure 10 shows that $f_{cf}(\infty)$ changes slowly as flow rate is increased.

In view of these results, curves such as those shown in Figure 9 can be used to calculate the in-place gas saturation in a reservoir, even when the porosity and permeability (or the parameter group Q/kh) are unknown. The partial pressure of CO_2 can be determined from down-hole pressure and temperature measurements and then the $f_{cf}(\infty)$ versus S_g curve for the correct temperature and partial pressure selected. A few degrees error in temperature or a few bar error in partial pressure of CO_2 will have a negligible effect on the results. Then a measurement of $f_{cf}(\infty)$ during a constant-rate production test can be used to obtain the in-place gas saturation. The only drawback of this process is that the shape of the $f_{cf}(\infty)$ versus S_g curves depends on the choice of relative permeability curves. For example, if the down-hole temperature and partial pressure of CO_2 in a well were measured as 260°C and 10 bar, respectively and if a measurement of $f_{cf}(\infty)$ gave a value of 5%, then in Figure 9 would give values of S_g of approximately 0.13 for the SGB curves, and 0.30 for the Corey curves. The difference between these two results cannot be easily resolved by measuring $H_f(\infty)$ and using plots such as those shown in Figure 6. The flowing enthalpy is determined, as equation (4) shows, by the flowing CO_2 mass fraction independently of the relative permeabilities. A simple calculation shows that for $S_g = 0.13$, the ratio $k_{rg}/k_{r\ell}$ for the SGB curves is 0.69 and for $S_g = 0.30$, $k_{rg}/k_{r\ell} = 0.64$ for the Corey curves. The corresponding flowing enthalpies are 1253.6 and 1247.4 KJ/kg, respectively. Therefore at very low flow rates the stable flowing enthalpies are virtually indistinguishable.

If a number of tests are performed and the rise in flowing enthalpy measured in each case, some progress can be made but only if estimates of porosity and permeability are available. Then plots such as those given by Bodvarsson et al.[13] can be used to distinguish between the two cases. Flowing enthalpy will increase much more rapidly with increase in flow rate for the case of $S_g = 0.3$ than for the case of $S_g = 0.13$. However, in determining the correct scale for flow rate, it is necessary to know permeability; and in choosing the relevant curve to match, porosity must be known.

Grant[19] showed that for a gas-dominated system (immobile water phase) the simultaneous measurement of stable flowing mass fractions of two gases (CO_2 and H_2S in that case) could be used to deduce the gas saturation of the reservoir. Further work is required to test the applicability of his method to all two-phase reservoirs and to investigate its accuracy for gas-dominated systems.

In summary, the measurement of stable flowing CO_2 mass fraction enables vapor saturation to be determined for each set of relative permeability curves being considered. Distinguishing between the different options requires knowledge of porosity and permeability and observation of the change in stable flowing enthalpy with flow rate.

WELL-TEST ANALYSIS

Pritchett et al[5] showed that the addition of quite small amounts of CO_2 produces large changes in the pressure drop during a constant-rate well test. In the example considered by Pritchett et al., the initial total pressure and temperature were fixed while the CO_2 content was varied. A change in CO_2 content is accompanied by large changes in the initial gas saturation (see Fig. 2) and this is probably the cause for most of the differences in mobility noted by Pritchett et al. In order to examine the effects of CO_2 on the pressure decline when the gas saturation effects are removed, a number of simulations were run with fixed initial temperature and gas saturation but different initial partial pressures of CO_2 and therefore different initial total pressures. A typical set of results is shown in Figure 11. The presence of CO_2 causes two effects. First, degassing causes a more rapid pressure decline at early times and the lower flowing enthalpy with CO_2 present causes a slower decline of temperature, and therefore pressure, at later times. The different slopes shown in Figure 11 (10.9 bar/cycle for $p_c = 0$ and 4.6 bar/cycle for $p_c = 30$ bar) result from differences in gas saturation in the gassy flow caused by differences in flowing enthalpy. Even if the reservoir fluid is correctly identified as two-phase, Figure 11 indicates that significant errors could easily be made in deducing kh from the slope of the semilog pressure plot unless accurate information on the CO_2 content is available.

NATURAL STATE STUDIES

In order to determine the effect of CO_2 on the natural thermodynamic state of geothermal systems, numerical studies of a simple vertical column model were carried out. The model consisted of two zones, a "caprock" extending from ground surface to 300 m with a permeability of 0.5 md and an underlying 700-m-thick reservoir zone with a permeability of 20 md. The thermal conductivity of both zones was assumed to be 2.0 W/m.°C; other reservoir paramaters such as porosity and heat capacity (storage type parameters) do not affect steady-state results. Heat and mass were injected at the base of the model in order to simulate an upflow zone in a geothermal system. Ambient conditions were prescribed at ground surface (T=10°C, P=1 bar).

In the first series of simulations the system was modeled without CO_2; mass and energy flow through the system adjusted until a small two-phase zone developed in the upper portion of the reservoir (shown by the shaded zone in figure 12). This occurred when 2.0 kg/s.km^2 of water, with an enthalpy of 1300 kJ/kg, was injected at the bottom of the model. Then, progressively larger and larger

quantities of CO_2 were added to the injected fluid; the results are shown in Figure 12. The figure shows that quite small quantities of CO_2 have a large effect on the thermodynamic state in the system. In the case of 1% flowing CO_2 mass fraction (corresponding to smaller in-place values), the boiling zone spreads throughout the whole column. For still higher concentrations of CO_2, gas saturation increases at the base of the caprock and throughout most of the caprock. In the reservoir, the gas saturation is close to the residual steam saturation. It is interesting to note that the gas saturation has two maxima, one near the base of the caprock and one at a shallow depth close to ground surface. The shape of the gas saturation distribution is related to the partial pressure of CO_2 shown in Figure 13. The local maximum in p_c at a depth of approximately 180 m corresponds to a temperature there of approximately 180°C, which is the temperature at which the solubility of CO_2 in water reaches a minimum (see Fig. 1). For temperatures on either side of this minimum, the partial pressure of CO_2 must drop and the gas saturation must rise to preserve a constant vertical heat and CO_2 flux through the column. It is of interest to note that Figures 12 and 13 predict high gas content in fluids at shallow depths. This is consistent with field observations from some wells at the Krafla geothermal field in Iceland (V. Stefansson, personal communication, 1982). The results obtained depend on the choice of relative permeability curve, as shown in Figure 12. The higher gas phase mobility of the X-curves and the SGB curves, in comparison with the Corey curves, implies that a lower gas saturation is required to transport the same quantity of CO_2.

MODELS OF OHAAKI

The Ohaaki (formerly Broadlands) geothermal field in New Zealand has been under investigation for over two decades. To date over 40 wells have been drilled in the area, mostly during the period 1966-1970[14]. The wells have identified the presence of a high-temperature (up to 300°C) two-phase reservoir[10] with substantial quantities of non-condensible gases (primarily CO_2)[9]. Power production of 100 MW_e is scheduled to start in 1985.

At Ohaaki there is little apparent geothermal activity at the surface. There is one major hot spring in the area, the Ohaaki Pool, which discharged approximately 10 kg/s before significant well discharges began. A number of small steam vents are also present. During the period 1966-1971 many of the Ohaaki wells were discharged with a total of 35 Mt of fluids removed[9]. This caused significant pressure drawdowns in the field (up to 20 bar); the pressure recovery is still not complete. The pressure data along with enthalpy and CO_2 data from the discharging wells are used in the following analysis of the Ohaaki reservoir.

The first model of Ohaaki investigated was a lumped-parameter model consisting of one reservoir block adjacent to a very large recharge block. The initial state selected was the same as that used previously by Grant[9] and Zyvoloski and O'Sullivan[7] in similar modeling studies, namely, $p = 62$ bar, $S_g = 0.2$, and $p_c = 15$ bar. Reservoir rock parameters were also taken from these previous studies with density of rock 2500 kg/m^3, specific heat of rock 900 J/kg.°C, and porosity 0.15. The monthly production figures[14] for wells BR 2, 3, 8, 9, 11, 13, 17-23, 25, were lumped together to give a total discharge history as shown in Figure 14. The volume of the reservoir block and the permeability connecting the reservoir and recharge blocks were then varied until the calculated pressure drawdown and recovery matched the observed data. Varying the reservoir permeability is equivalent to varying the recharge coefficient in the pressure-dependent recharge term used in previous investigations[7,9]. The "best fit" reservoir volume is 0.82×10^9 m^3 and permeability 82×10^{-15} m^2. This volume is larger than that found in previous studies[7,9] but a more accurate production history was used in the present study. The comparison between calculated pressure drawdowns and the observed ones is shown in Figure 14. The agreement is good, but for production enthalpy and production CO_2 content the match is poor as should be expected from such a crude model. The long-term response of a lumped-parameter model such as that considered is almost entirely dependent on the recharge assumptions. The large recharge block ensures that the properties of the recharge fluid (enthalpy and CO_2 content) remain constant with time. To allow the recharge fluid properties to vary realistically requires the use of some form of distributed parameter model. The first of these considered was a vertical column model. This model matches both the thermodynamic conditions of the field in the natural state and the reservoir response to exploitation reasonably well. The model used is shown in Figure 15. The primary reservoir at Ohaaki is located in the Waiora and breccia formations, although considerable horizontal permeability is also found in the rhyolite[20]. The basement rock at Ohaaki is the ignimbrite. We use a total of 10 elements in the natural state simulations; the top element is maintained at ambient conditions (T = 10°C, p = 1 bar). Heat and mass (H_2O and CO_2) are injected into the bottom element (ignimbrite).

In simulating the natural state of geothermal reservoirs, mass and heat flows to surface manifestations must be carefully modeled. We use a deliverability model to calculate the mass of CO_2 and water discharged at the surface springs. Mathematically, the model is:

$$Q = PI \left(\frac{k_\ell}{\nu_\ell} + \frac{k_g}{\nu_g} \right) (p - p_{cr}),$$

where PI is the productivity index of the natural vents, and p_{cr} is the critical pressure, i.e., the minimum pressure required for discharge to occur. We use critical pressures of 26 and 22 bar for mass flow to the Ohaaki Pool and the surface steam vents, respectively. The use of a deliverability model for fluid flow to the surface springs is necessary, because as the pressures fall in the reservoir during exploitation, the mass flow to the springs will decline or disappear altogether.

In the natural-state simulations, we varied the heat/mass upflow and the vertical permeability distributions until a reasonable match was obtained with observed pressures and temperatures. The X relative permeability curves, with residual liquid and steam saturations of 0.3 and 0.05, respectively, were used exclusively. The productivity indices

for mass flow from the rhyolite to Ohaaki Pool and surface steam vents were adjusted to give observed mass flows (10 kg/s to the Ohaaki Pool and an estimated 3 kg/s to surface steam vents). After reasonable natural state results were obtained, the 1966-1971 exploitation test of the Ohaaki field was modeled. The exploitation simulations put additional constraints on vertical permeabilities within the system, necessitating additional iterations between the natural-state model and the exploitation model. The iteration process was continued until reasonable results were obtained for both the natural state and the system behavior under exploitation. In the best natural-state model obtained, the parameters shown in Table 2 were used. The total mass flow through the system was 18.625 kg/s with a flowing mass fraction of CO_2 of .06. The heat flow through the system was 24.5 MW_t. Most of this mass and heat is discharged to surface springs. The vertical permeability distribution appears reasonable; permeability is low in the ignimbrite, high in the main reservoir (Waiora and breccia formations), and low between the rhyolite and the Waiora formations. This agrees well with interference test data from the field[20].

Comparisons between calculated and observed[10,21] pressure and temperature profiles are shown in Figures 16 and 17, respectively. The agreement is excellent. Figure 18 shows the calculated gas saturation and partial pressure of CO_2 profiles, indicating a monotonic increase in the partial pressure of CO_2 with depth. The partial pressure of CO_2 in the main reservoir is 15-25 bar. The gas-saturation profile shows very low values in the main reservoir region (close to the residual gas saturation of 0.05). The gas-saturation profile in the rhyolite and Huka Falls formation reflects the combination of two effects: rather high gas saturations are necessary to enable the required through-flow of CO_2, and the low gas saturation at a depth of 300 m is a result of gas escaping to surface manifestations (Ohaaki Pool and steam vents).

The best-fit steady-state pressure, temperature, and CO_2 distribution were then used as initial conditions for simulations of the exploitation and recovery of the Ohaaki reservoir during 1968-1974. In the exploitation model, very large recharge blocks were added adjacent to each of the reservoir blocks. These recharge blocks cause a recharge flow into each reservoir block proportional to the pressure drop there. The large size of the recharge block maintains the initial values for the enthalpy and CO_2 content of the recharge.

For this vertical-column model the production data used for the single-block model was classified as either deep or shallow, using information on feed zones given by Grant[21]. The deep production was assigned to block 9 (BR 9, 13, 17-20, 22, 23, 25), and the shallow production to block 7 (BR 2, 3, 8, 11, 21). In calibrating the model, the parameters which can be varied without any change to the initial steady-state model are the porosity of each block and the horizontal permeability between the reservoir and recharge blocks. Two general cases were considered. In Case I, the porosity and horizontal permeability in the production zone (blocks 7, 8, 9) were assumed to be uniform. In Case II, the porosity and horizontal permeability were allowed to be different in blocks 7 and 9. The nonuniformity of horizontal permeability in Case II allows the high-permeability zone at the contact between the rhyolite and the Waiora formation[20] to be represented.

In both Case I and Case II, the porosities and horizontal permeabilities were then adjusted to give a good match to the pressure response shown in Figure 14. The pressure in block 9, was used as an average reservoir pressure to compare with recorded data[9]. By running only a few simulations, it was possible to obtain a very good pressure match, similar to that for the single-block model shown in Figure 14. The most interesting results from the model, however, are the production enthalpy data. For Case I (uniform horizontal permeability), the production enthalpy is too high from the shallow wells. These results confirm the postulated[20] high horizontal permeability just below the rhyolite. Shallow well enthalpies are still overpredicted by the model. The mass fraction of CO_2 in the production zone is shown in Figure 20. The agreement is reasonable, but these results are sensitive to the choice of the relative permeability functions. Further simulations with a colder recharge into the shallow production zone produced a better match to the observed enthalpy response. However the corresponding match to the CO_2 data was not as good.

The vertical-column model of Ohaaki could be improved with further experimentation with parameters. For example, it is probable that a slightly lower vertical permeability in the lower production zone (blocks 8 and 9) would give a better match to the deep production enthalpy. However, the productive enthalpy and CO_2 data vary from well to well[14], and to produce a good match to production enthalpies and CO_2 mass fractions the production wells at Ohaaki must be modeled individually. Such a model has been developed for the Krafla geothermal field in Iceland by two of the present authors[22,23].

CONCLUSIONS

The results of this investigation show that the effects of a noncondensible gas such as CO_2 on geothermal reservoir behavior can be extremely important. In the natural state, CO_2 increases the size of the boiling zone considerably. During exploitation, the gas escapes rapidly, leading to a large early pressure drop.

The presence of CO_2 significantly affects the results of transient well tests. The pressure response is faster at early times because of degassing and slower at later times because of a reduced flowing enthalpy. The measurement of the CO_2 mass fraction in the produced fluid during a well test can be used to deduce the in-place gas saturation in the reservoir if the relative permeabilities are known.

The preliminary modeling of the Ohaaki geothermal field reported here has greatly assisted in understanding the structure of the reservoir by establishing a vertical permeability distribution which produces consistent pressure and temperature distributions. The brief investigation of production models has given useful insight into the horizontal permeability at Ohaaki and provides a basis for more complete modeling studies.

The single-block and vertical-column models can both provide reasonable matches to the field data from the 1968-1974 period, but they should not be used for long-term future predictions because their representation of recharge is not sufficiently accurate.

NOMENCLATURE

f_{cf}	flowing CO_2 mass fraction
$f_{c\ell}$	CO_2 mass fraction in liquid
f_{cg}	CO_2 mass fraction in gas
$f_{cf(\infty)}$	stabilized flowing CO_2 mass fraction
h	reservoir thickness, m
H_f	flowing enthalpy, kJ/kg
H_ℓ	enthalpy of liquid phase, kJ/kg
H_v	enthalpy of gas phase, kJ/kg
$H_{f(\infty)}$	stabilized flowing enthalpy, kJ/kg
k	permeability, md
k_h	horizontal permeability, md
$k_{r\ell}$	relative permeability for liquid
k_{rg}	relative permeability for gas
k_v	vertical permeability, md
ν_f	total kinematic viscosity, m^2/s
ν_ℓ	kinematic viscosity of liquid, m^2/s
ν_g	kinematic viscosity of gas, m^2/s
p	pressure, bars
p_c	partial pressure of CO_2, bars
p_{co}	initial partial pressure of CO_2, bars
p_{cr}	critical pressure in deliverability formula, bars
PI	productivity index, m^3
ϕ	porosity
Q	mass flow rate, kg/s
S_g	gas saturation
S_{go}	initial gas saturation
T	temperature, °C
X_c	mole fraction of CO_2

ACKNOWLEDGEMENTS

The authors thank M. J. Lippmann and C. Doughty of Lawrence Berkeley Laboratory for critical review of this work. The first author also acknowledges financial support by the New Zealand University Grants Committee through the Claude McCarthy Fellowship.

This work was supported by the Assistant Secretary for Conservation and Renewable Energy, Office of Renewable Technology, Division of Geothermal and Hydropower Technologies of the U. S. Department of Energy under Contract No. DE-AC03-76SF00098.

REFERENCES

1. Pruess, K., 1982, "Development of the general purpose simulator MULKOM," Annual Report, Earth Sciences Division, Lawrence Berkeley Laboratory, Berkeley, California.

2. Pruess, K., and Schroeder, R. C., 1980, "SHAFT79, User's Manual," Lawrence Berkeley Laboratory Report LBL-10861.

3. Zyvoloski, G. A., and O'Sullivan, M. J., 1980, "Simulation of a gas-dominated, two-phase geothermal reservoir," Soc. Pet. Eng. J., 20(1), 52-58.

4. Sutton, F. M., and McNabb, A., 1977, "Boiling curves at Broadlands field, New Zealand," N.Z.J. Sci., 20, 333-337.

5. Pritchett, J. W., Rice, M. H., and Riney, T. D., 1981, "Equation-of-state for water-carbon dioxide mixtures: Implications for Baca reservoir," Report prepared by Systems, Science and Software, La Jolla, California.

6. Atkinson, P. G., Celati, R., Corsi, R., and Kucuk, F., 1980, "Behavior of the Bagnore steam/CO_2 geothermal reservoir, Italy," Soc. Pet. Eng. J., 20(4), 228-238.

7. Zyvoloski, G. A., and O'Sullivan, M. J., 1978, "A simple model of the Broadlands geothermal field," N.Z.J. Sci., 21, 505-510.

8. Zyvoloski, G. A., and O'Sullivan, M. J., 1978, "Simulation of the Broadlands geothermal field, New Zealand," Proc. 4th Workshop on Geothermal Reservoir Engineering, Stanford, 332-342.

9. Grant, M. A., 1977, "Broadlands - A gas-dominated geothermal field," Geothermics, 6, 9-29.

10. Bixley, P. F., 1976, "Broadlands geothermal area - underground temperatures, and some thoughts on the reservoir(s) and future drilling," Geothermal Circular P.F.B.1, Ministry of Works and Development, Wairakei.

11 Grant, M. A., 1977, "Permeability reduction factors at Wairakei," AIChE-AIME Heat Transfer Conf. Paper 77-HT-52.

12 Horne, R. N., and Ramey, H. J., Jr., 1978, "Steam-water relative permeability from production data," G.R.C., 2, 291-294.

13 Bodvarsson, G. S., O'Sullivan, M. J., and Tsang, C. F., 1980, "The sensitivity of geothermal reservoir behavior to relative permeability parameters," Proc. 6th Workshop on Geothermal Reservoir Engineering, Stanford, 224-237.

14. Ministry of Works and Development, 1977, "Broadlands Geothermal Investigation Report," M.W.D., Wellington, New Zealand.

15. Grant, M. A., 1977, "Gas content in Broadlands deep water," Geothermal Circular MAG15, Applied Mathematics Division, D.S.I.R., Wellington.

16. Corey, A. T., 1972, "Mechanics of heterogeneous fluids in porous media," Water Resour. Pub., Fort Collins, Colorado.

17. Sorey, M. L., Grant, M. A., and Bradford, E., 1980, "Nonlinear effects in two-phase flow to wells in geothermal reservoirs," Water Resour. Res., 16(4), 767-777.

18. O'Sullivan, M. J., 1981, "A similarity method for geothermal well test analysis," Water Resour. Res., 17(2), 390-398.

19. Grant, M. A., 1979, "Water content of the Kawah Kamojang geothermal reservoir," Geothermics, 8, 21-30.

20. Grant, M. A., 1982, "The interaction of the Ohaaki Reservoir with surrounding fluid," Geothermal Circular MAG37, Applied Mathematics Division, D.S.I.R., Wellington.

21. Grant, M. A., 1980, "Changes in fluid distribution at Ohaaki," Proc. N. Z. Geotherm. Workshop, University of Auckland, 69-74.

22. Bodvarsson, G.S., Pruess, K., Stefansson, V., and Eliasson, E.T., 1982, A summary of modeling sutdies of the Krafla geothermal field, Iceland, Proceedings of the 7th annual meeting of the Geothermal Resources Council, Portland, Oregon, Oct. 24-27, 1983.

23. Pruess, K., Bodvarsson, G.S., Stefansson, V. and Eliasson, E.T., 1982, The Krafla geothermal field, Iceland, 4. Well by well model and reservoir depletion, to be submitted to Water Resources Research

24. Ellis, A. J., and Goulding, R. M., 1963, "The solubility of carbon dioxide above 100°C in water and in sodium chloride solutions," Am. J. Sci., 261, 47-60.

25. Malinin, S. D., 1959, "The system water-carbon dioxide at high temperatures and pressures," Geokhimiya, 10, 1523-1549.

26. Takenouchi, G., and Kennedy, G. C., 1964, "The binary system H_2O-CO_2 at high temperatures and pressures," Am. J. Sci., 272, 1055-1074.

27. Gibb, R. E., and Van Ness, H. S., 1971, "Solubility of gases in liquids in relation to the partial molar volumes of the solute. Carbon dioxide-water," Ind. Eng. Chem. Fundam., 10(2), 312-315.

28. Vargaftik, N. B., 1975, "Tables on the Thermophysical Properties of Liquids and Gases," 2nd Edition, John Wiley and Sons, Inc., New York.

APPENDIX

The thermodynamic package used in this study is based on the model suggested by Sutton and McNabb[4] and used subsequently by others[3,5]. Various formulae are used which are only exact for mixtures of ideal gases or nonideal gases at low pressures. For conditions of interest in geothermal reservoirs, say 10°C < T < 310°C, 1 bar < p < 120 bar, 0 < p_c < 50 bar, the errors in using some of these formulae remain uncertain, but for those where comparison with tabulated data is possible the errors are less than 5%.

The primary variables used are total pressure, p, temperature, T, and partial pressure of CO_2, p_c, for single-phase conditions. T is replaced by gas saturation, S_g, for two-phase conditions. For compressed liquid conditions the interpretation of p_c is that it is the pressure required to keep all the CO_2 present in solution at the prevailing temperature.

The mass and heat balance equations are non-linear, and are solved by MULKOM using Newton-Rapheson iteration. As the primary variables change during the iteration process, the thermophysical properties package must be capable of (i) recognizing the appearance and disappearance of phases, and (ii) providing all needed thermophysical parameters appropriate for the latest iterated values of the primary variables. We shall here outline how this is accomplished for the different phase compositions which may be present in the H_2O-CO_2 system.

Compressed liquid

Given p, T, and p_c, the boiling curve pressure $p_s(T)$ is first calculated from steam tables[1,2] and a check of p $p_s(T) + p_c$ is made to test for phase change to two-phase conditions. If p < $p_s(T) + p_c$, a change to the two-phase state is made and the gas saturation is initialized as a small non-zero quantity, $S_g = 10^{-6}$, say. Using standard H_2O thermodynamic formulae[1,2], the density of water, ρ_w, the viscosity of water, μ_w, and the enthalpy of water, H_w, are calculated. The mole fraction of CO_2 in solution, x_c, is calculated using Henry's law in the form

$$x_c = p_c / {}^{\alpha}(T) \qquad \text{(A1)}$$

The temperature-dependent coefficient ${}^{\alpha}(T)$ is defined by a piece-wise quadratic fit to published data[24,25,26,27]. Approximations are involved in equation (A1) both in using partial pressure instead of fugacity, and in the application of the formula at other than very small concentrations. The mass fraction of CO_2 in the liquid $f_{c\ell}$ is then calculated from x_c in an obvious way. The enthalpy of gaseous CO_2, $H_c(p_c, T)$ and the heat of solution of CO_2, $H_{sol}(T)$ are calculated using a formula given by Sutton and McNabb[4] and a quadratic fit to data from Ellis and Golding[24], respectively. A comparison of the formula for H_c with tabulated data[28] shows the accuracy is better than 5% in the required range of interest. Then all the required parameters are calculated using the approximations

$$\rho_\ell = \rho_w \qquad \text{(A2)}$$

$$\mu_\ell = \mu_w \qquad \text{(A3)}$$

$$H_\ell = H_w(1 - f_{c\ell}) + (H_c + H_{sol})f_{c\ell} \qquad \text{(A4)}$$

Two-Phase

Given p, S_g, and p_c, first a phase-transition test is made by examining whether S_g satisfies the inequality $0 < S_g < 1$. For $S_g < 0$ or S_g 1, the transition to single-phase liquid or gas, respectively, is made. The partial pressure of steam in the gas phase is readily calculated using

$$p_s = p - p_c$$

and then the temperature $T(p_s)$ is calculated from a steam table formula[1,2]. For the liquid phase, ρ_ℓ, μ_ℓ, and H_ℓ are calculated as above. For the gas phase the enthalpy $H_c(P_c, T)$ and density of CO_2, $\rho_c(p_c, T)$ are calculated using formulae given by Sutton and McNabb[4]. The viscosity $\mu_c(p_c, T)$ is calculated using an approximation to tabulate

data[28] suggested by Pritchett et al.[5]. The density of steam $\rho_s(p_s)$, viscosity of steam $\mu_s(T)$, and enthalpy of steam $H_s(T)$ are obtained from steam tables[1,2]. Now all the gas phase parameters can be calculated using

$$\rho_g = \rho_s + \rho_c \tag{A5}$$

$$\mu_g = \mu_s(1 - f_{cg}) + \mu_c f_{cg} \tag{A6}$$

$$H_g = H_s(1 - f_{cg}) + H_c f_{cg} \tag{A7}$$

The mass fraction of CO_2 in the gas, f_{cg}, used above follows simply as

$$f_{cg} = \rho_c/\rho_g \tag{A8}$$

from the definition of density. Other authors[4,5] have suggested using

$$f_{cg} = p_c/p \tag{A9}$$

however, since an accurate formula is available for calculating f_{cg}, this approximation is unnecessary.

Single phase gas

Given p, T, and p_c, first the boiling pressure $p_s(T)$ is calculated and a test for phase transitions is made by checking the inequality $p < p_s + p_c$. If the calculated p and T give $p > p_s + p_c$, then a transition to two-phase conditions is made. The procedure for calculating ρ_g, μ_g, and H_g follows that described above for the two-phase conditions except that now in calculating ρ_s, μ_s, and H_s, formulae appropriate for the superheated steam region are used.

Table 1

FLOWING CO_2 MASS FRACTION DEPENDENCE ON POROSITY

Initial pressure = 52 bars
Initial partial pressure of CO_2 = 5 bars
Flow-rate = 0.1 kg/s.m

	CO_2 Mass Fraction f_{cf} (∞)		
Porosity	S_g = 0.1	S_g = 0.3	S_g = 0.5
0.05	0.277	2.705	9.200
0.0625	0.276	2.706	9.523
0.10	0.273	2.703	0.218
0.15	0.271	2.696	10.831
0.20	0.269	2.689	11.277

Table 2

DATA USED IN VERTICAL COLUMN OHAAKI MODEL

		Case I		Case II	
Block	k_v (md)	k_h (md)	ϕ	k_h (md)	ϕ
2	1.2	1.2	0.2	1.2	0.2
3	1.5	1.5	0.15	1.5	0.15
4	1.5	1.5	0.15	1.5	0.15
5	0.6	0.6	0.15	0.6	0.15
6	0.6	0.6	0.15	0.6	0.15
7	1.0	10.0	0.10	40.0	0.10
8	10.0	10.0	0.10	10.0	0.10
9	10.0	10.0	0.10	7.0	0.10
10	0.5	0.5	0.10	0.5	0.10

Heat/mass upflow

mass H_2O: 17.5 kg/s
mass CO_2: 1.125 kg/s
heat: 24.5 MW_t

Heat/mass flow to surface springs

Ohaaki Pool: mass H_2O: 9.18 kg/s
mass CO_2: 0.04 kg/s
heat: 9.12 MW_t
Steam vents: mass H_2O: 3.84 kg/s
mass CO_2: 0.74 kg/s
heat: 8.56 MW_t
Thermal conductivity: 2.0 W/m·°C
Rock density: 2500 kg/m^3
Heat capacity: 900 J/kg.°C
Cross sectional area: 1.0 km^2

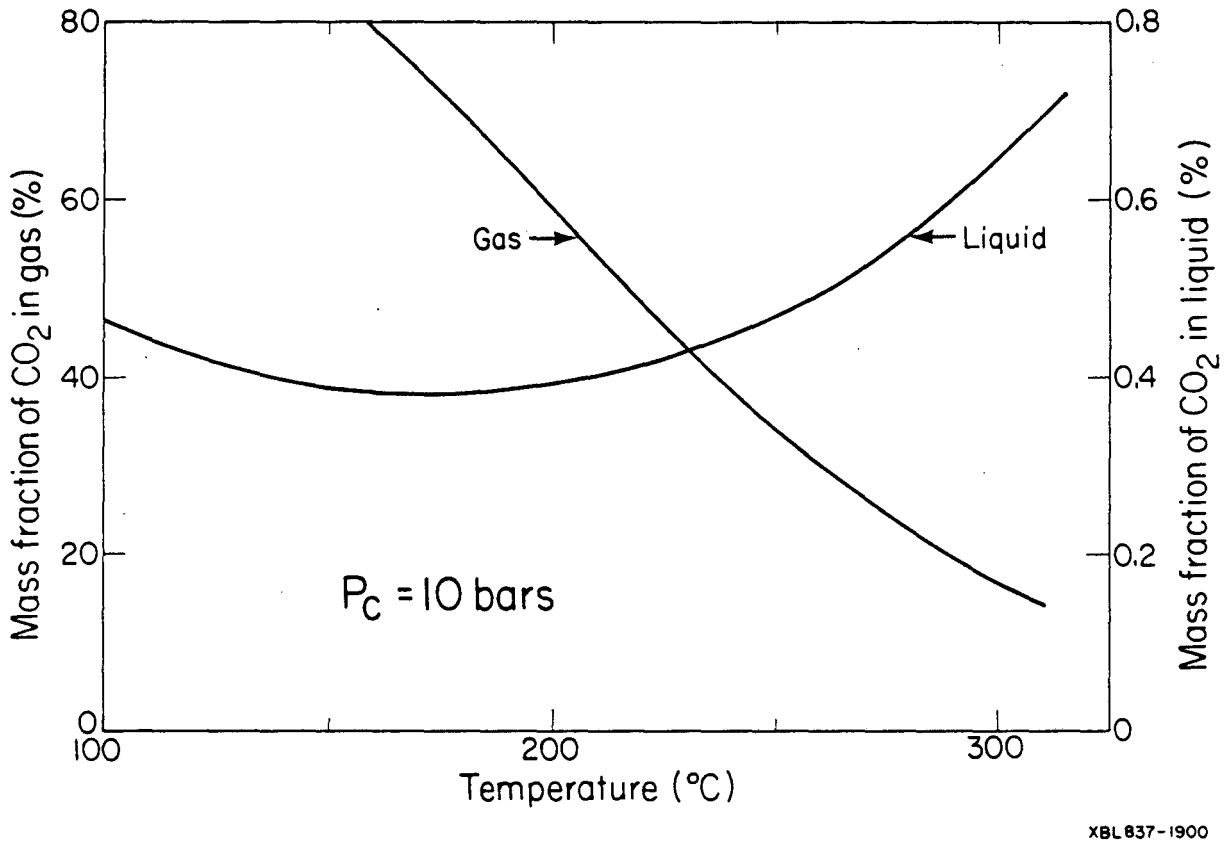

Figure 1. Mass fraction of CO_2 in liquid and gaseous phases.

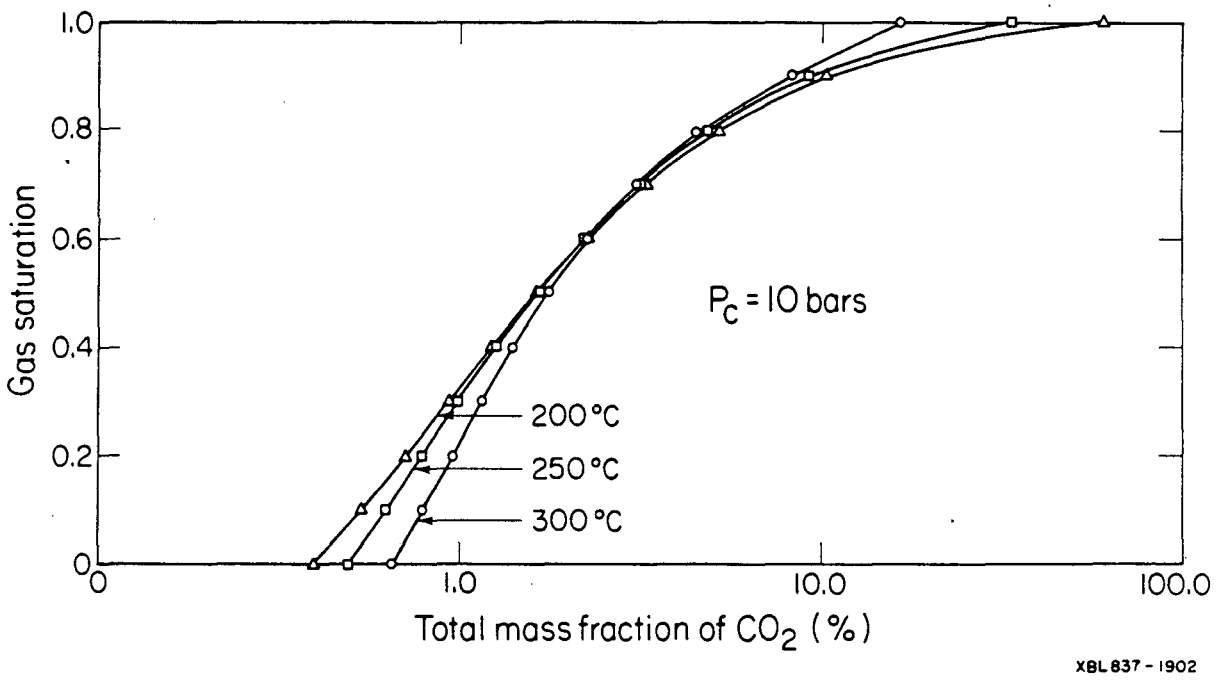

Figure 2. Variation of gas saturation with CO_2 content at constant temperatures and constant pressure (P_c = 10 bars).

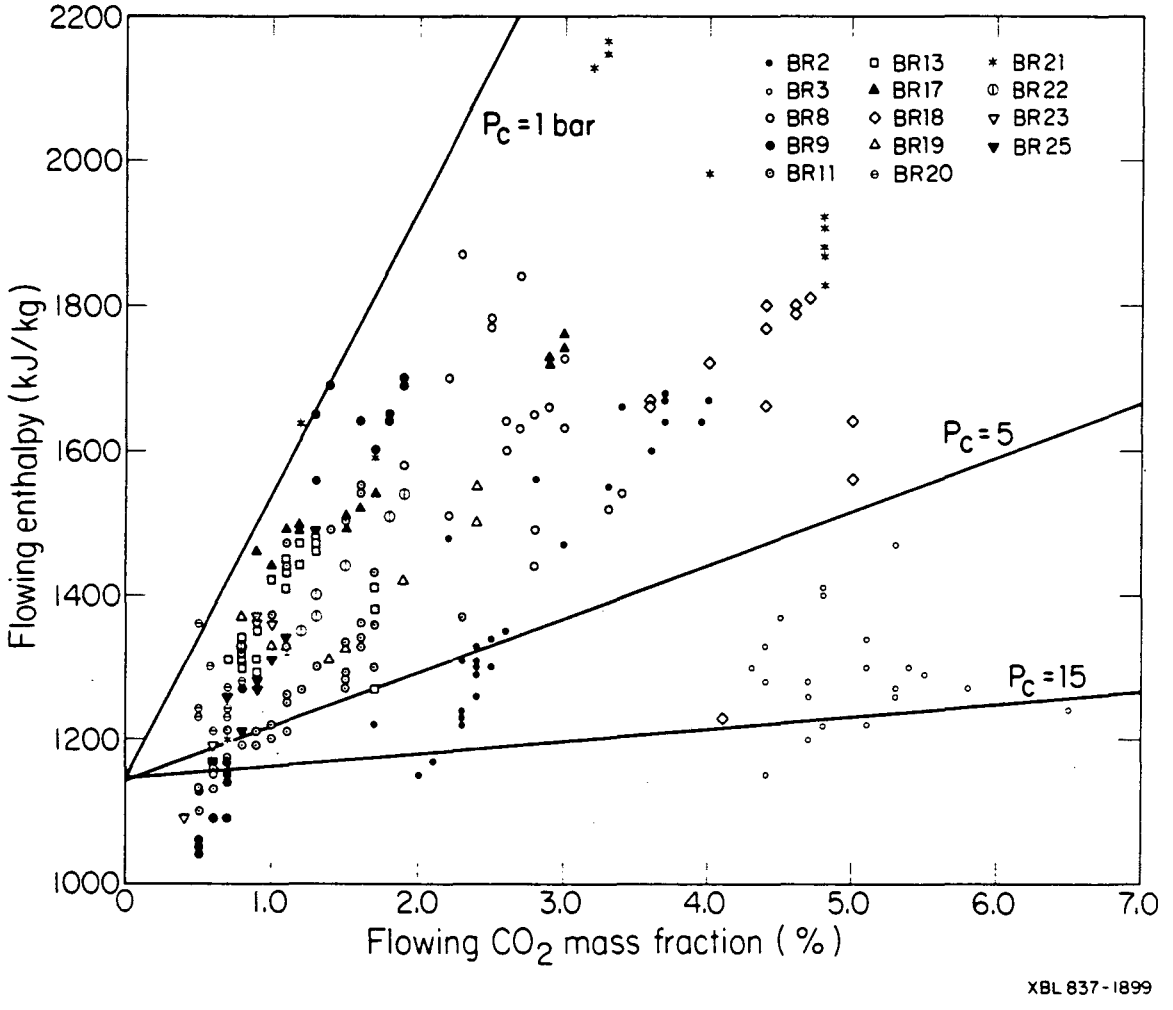

Figure 3. Variation of flowing enthalpy with flowing CO_2 mass fraction. Monthly production data from Ohaaki[14] is also known.

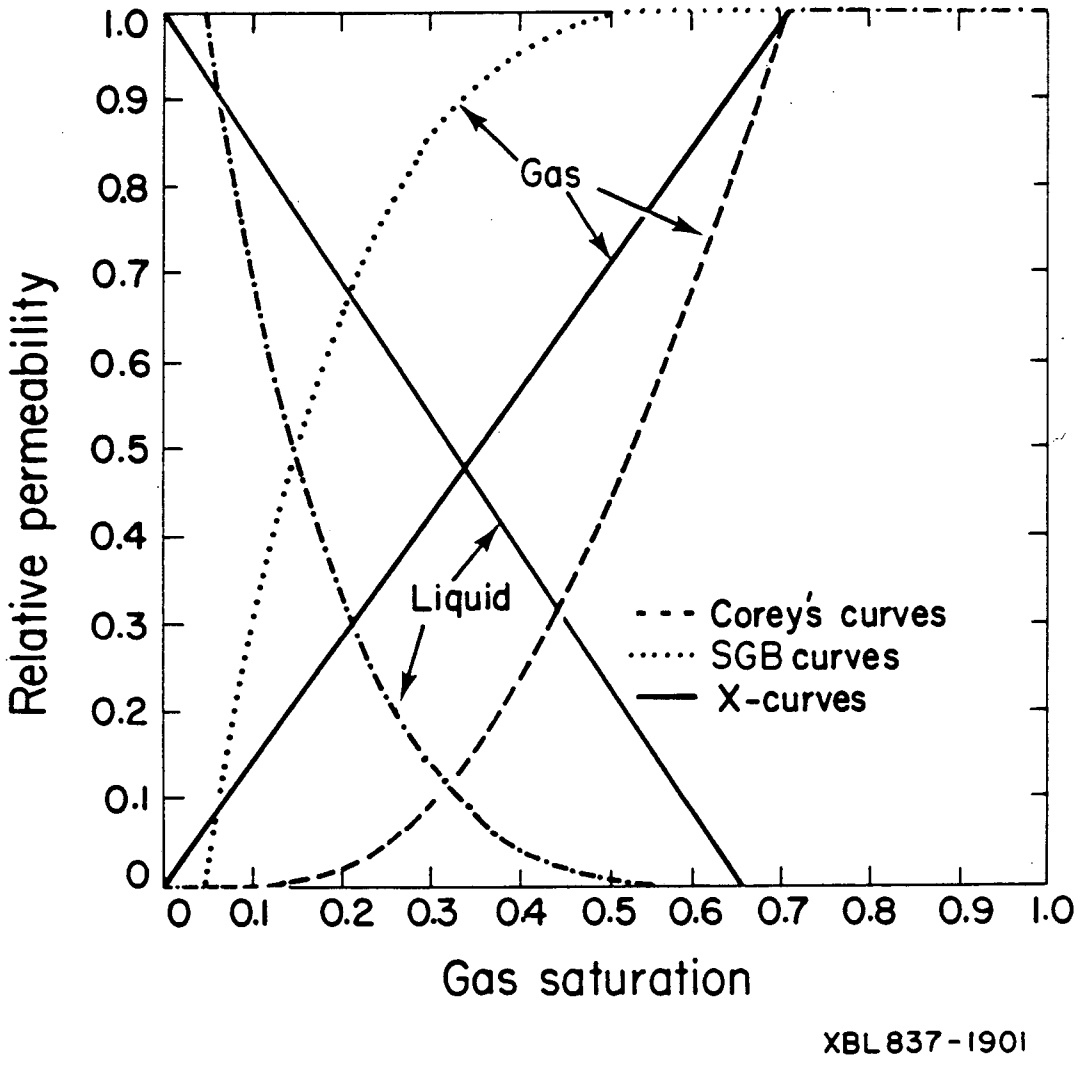

Figure 4. Relative permeability curves.

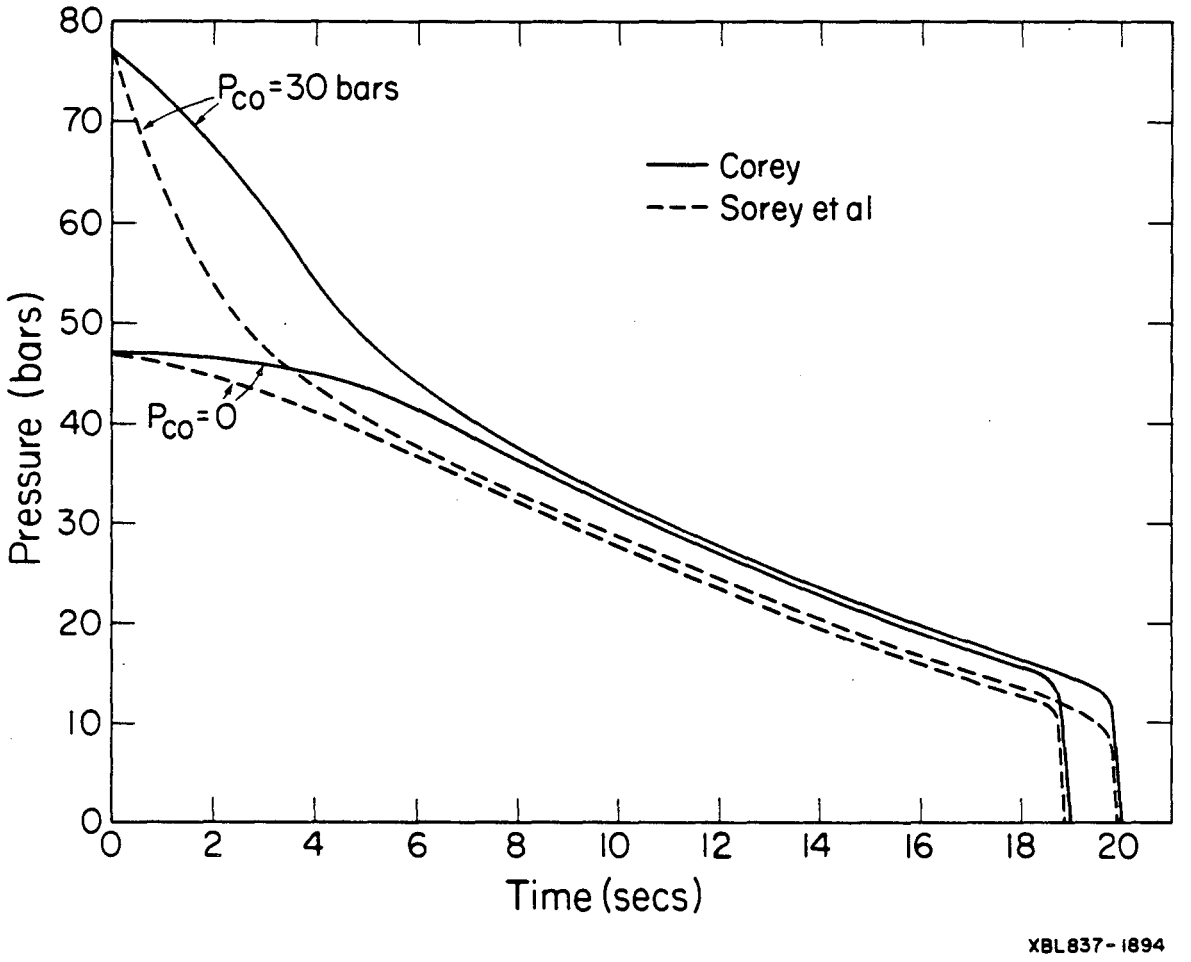

Figure 5. Depletion of a single-block reservoir.

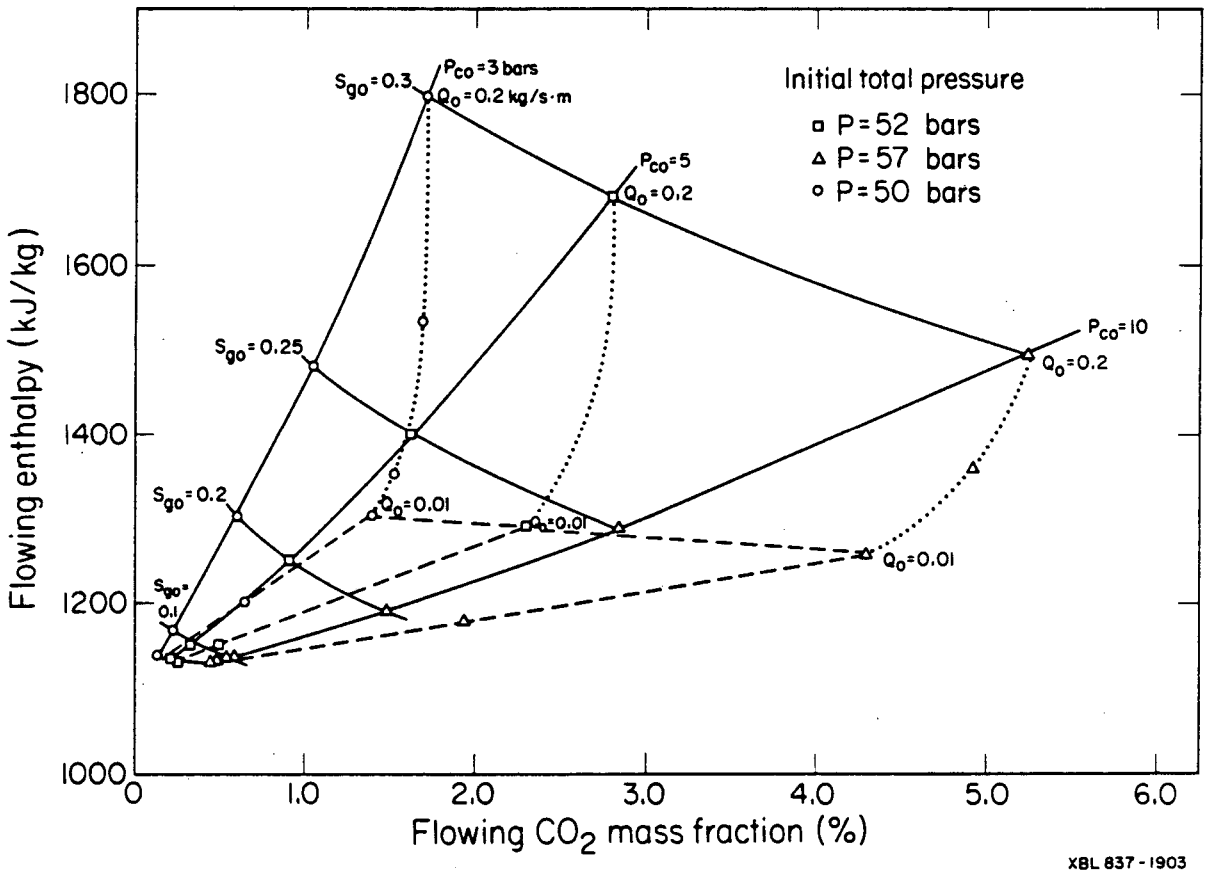

Figure 6. Stabilized flowing enthalpy versus stabilized flowing CO_2 content. S_{go} = initial gas saturation, P_{co} = initial partial pressure of CO_2, P = initial total pressure, Q = flow rate. Corey relative permeability curves.

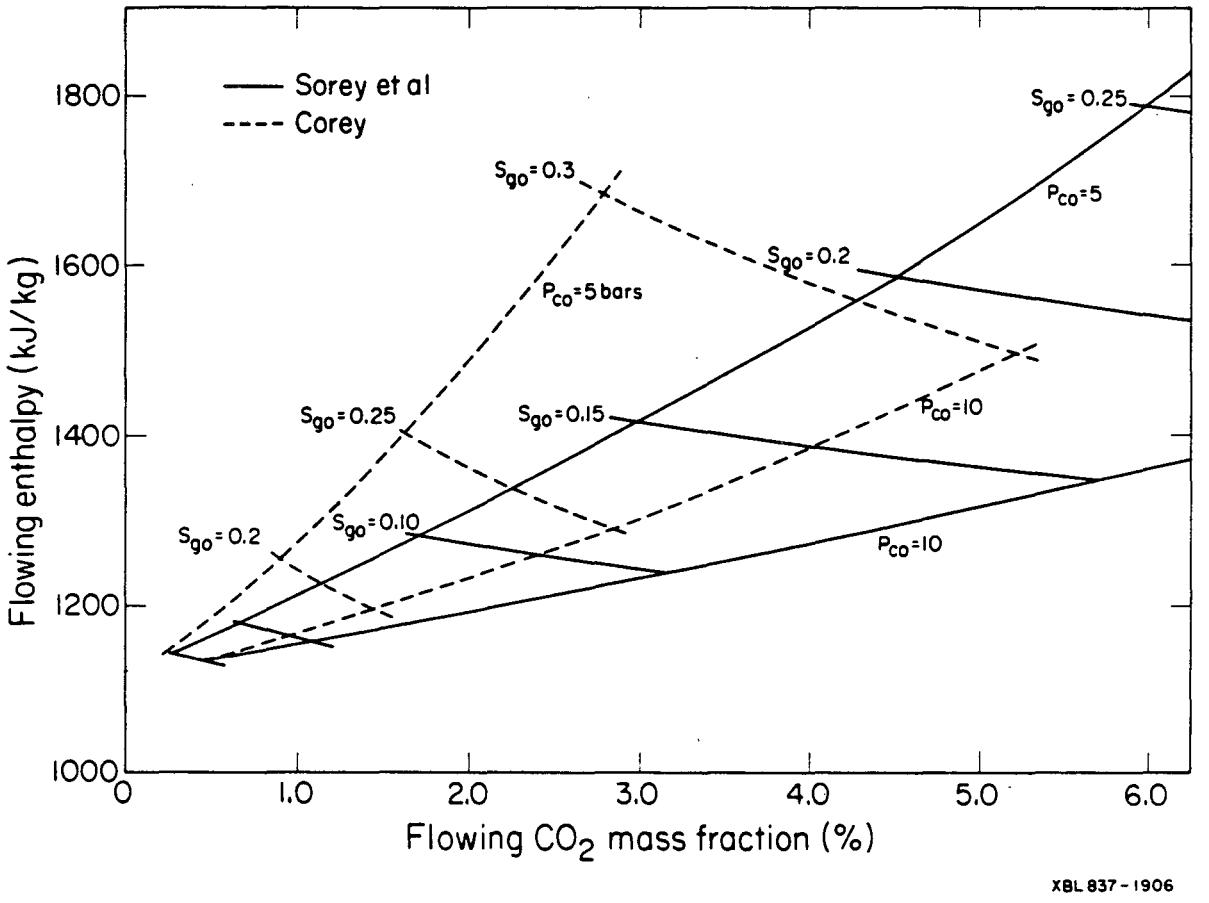

Figure 7. Stabilized flowing enthalpy versus stabilized flowing CO_2 content. Sorey et al. relative permeability curves.

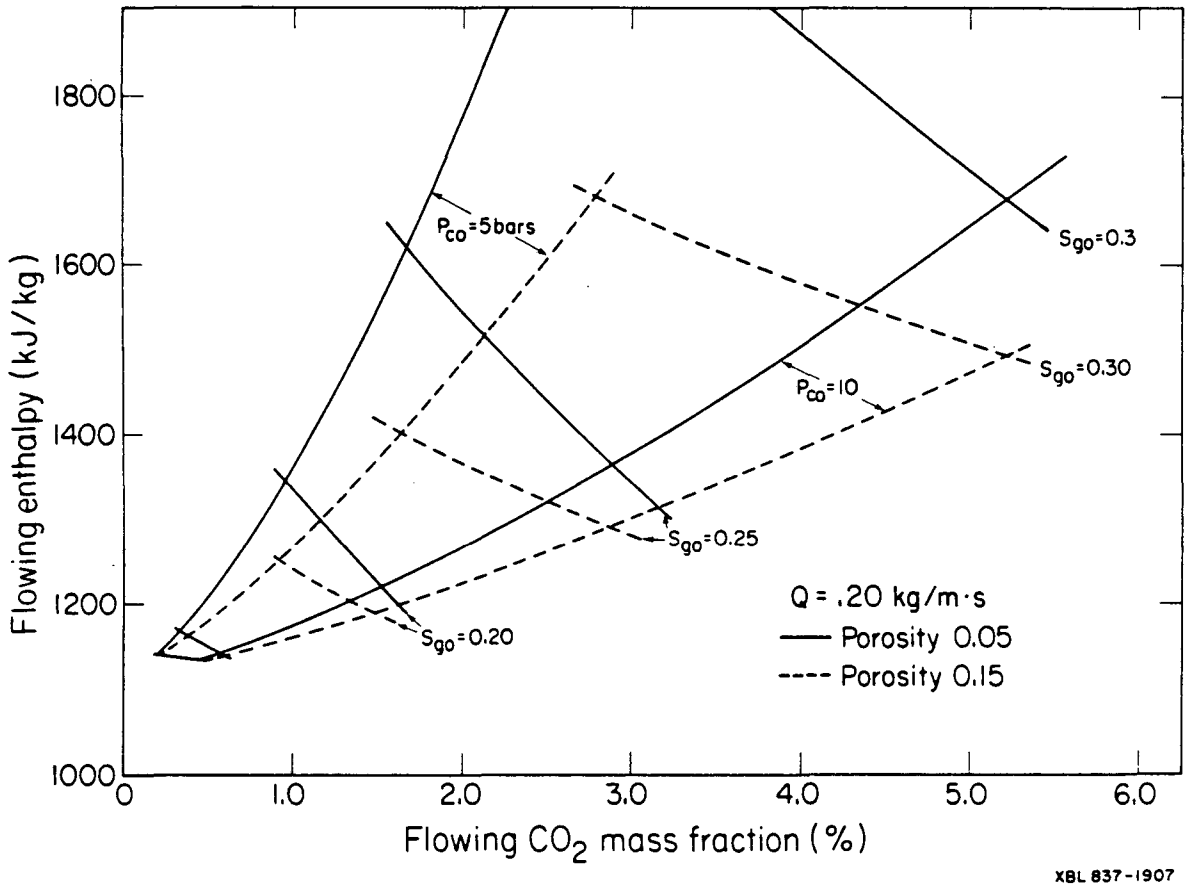

Figure 8. Stabilized flowing enthalpy versus stabilized flowing CO_2 mass fraction showing variation with porosity. Corey relative permeability curves.

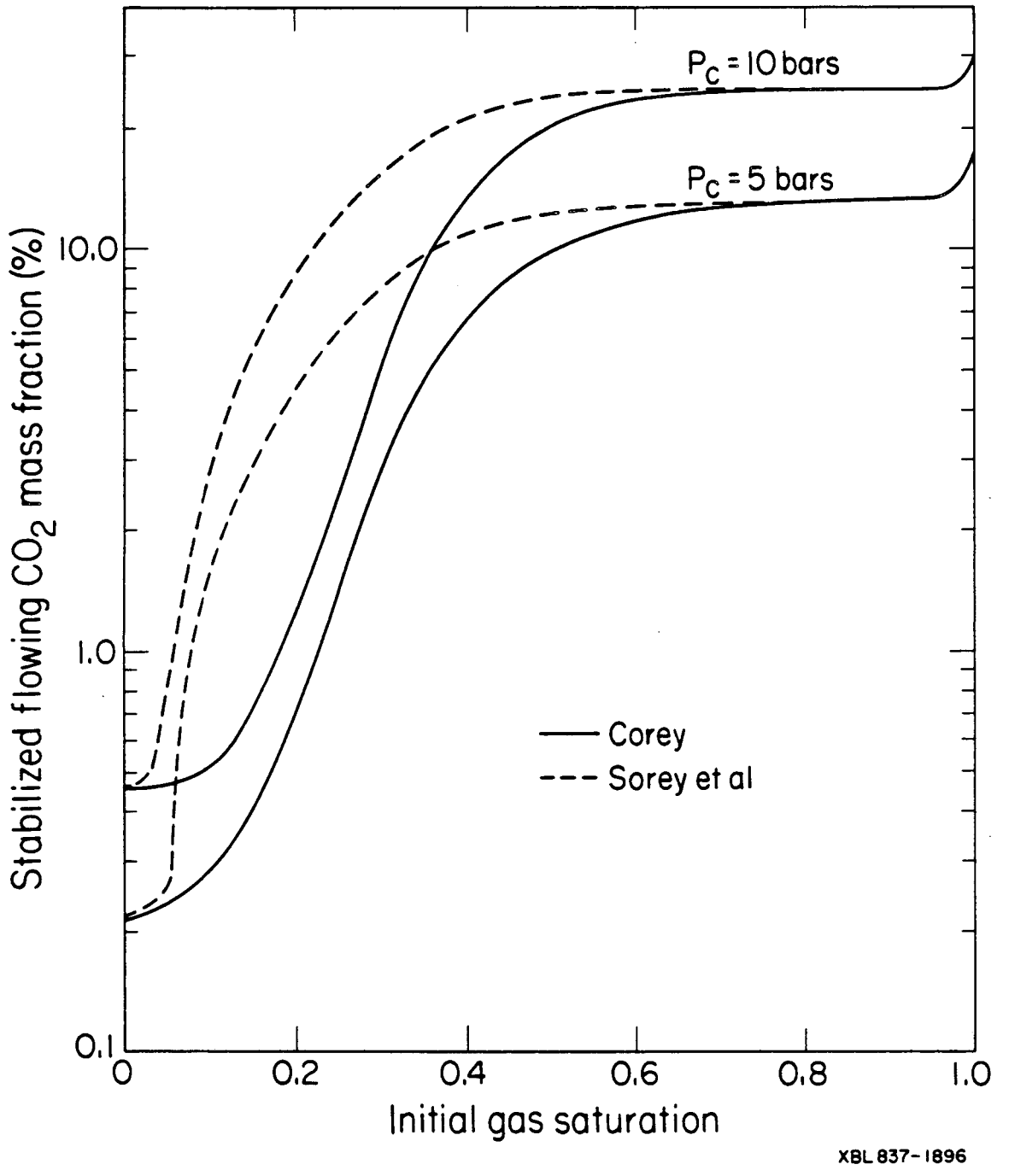

Figure 9. Variation of stabilized flowing CO_2 mass fraction with flow-rate.

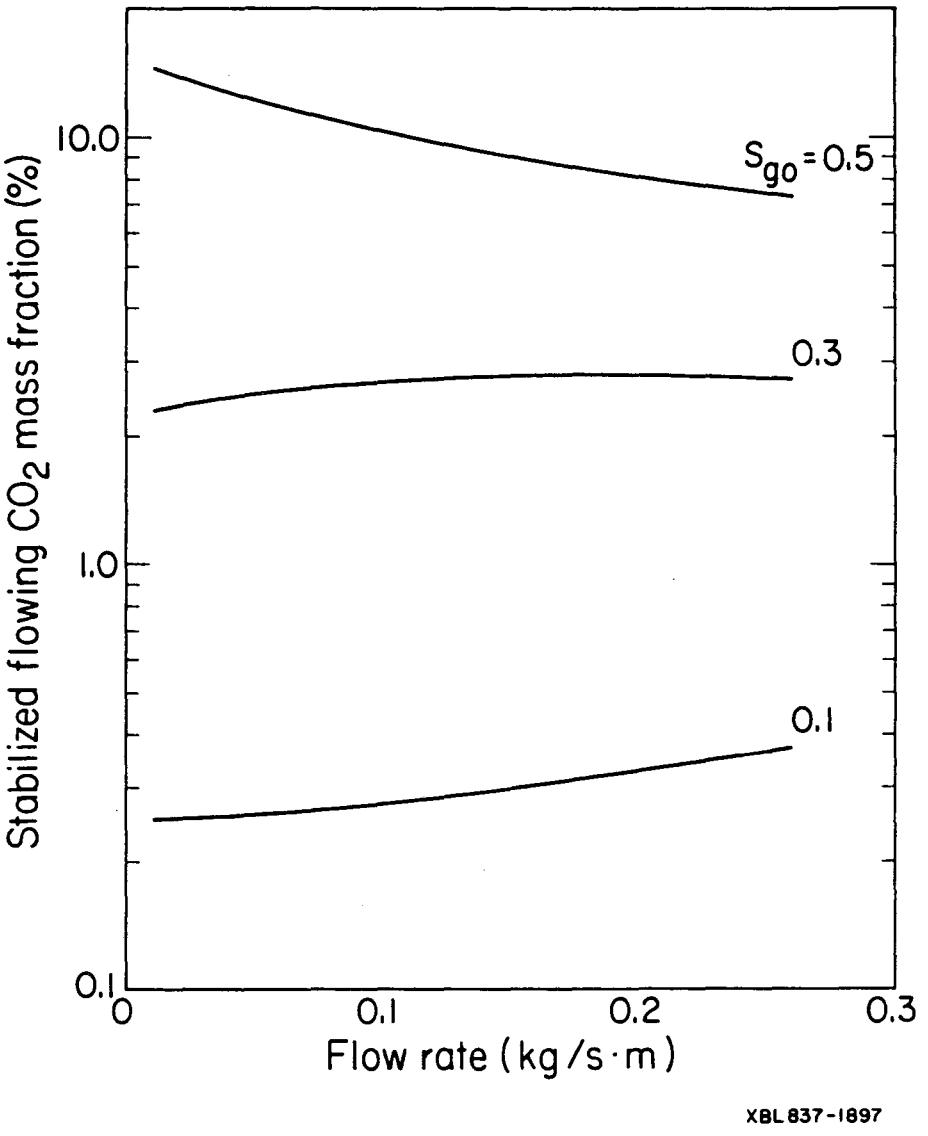

Figure 10. Variation of stabilized flowing CO_2 mass fraction with flow-rate.

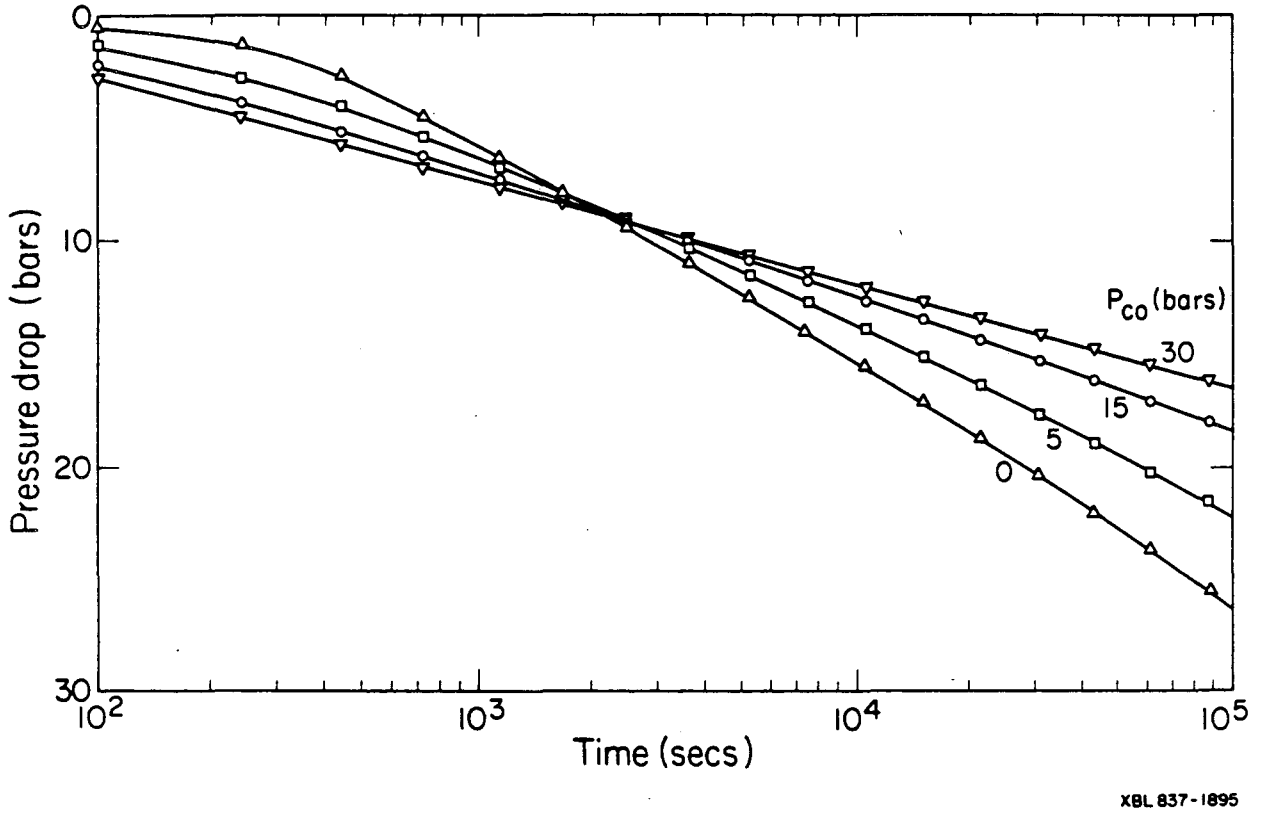

Figure 11. Typical pressure decline curves for a constant rate drawdown test.

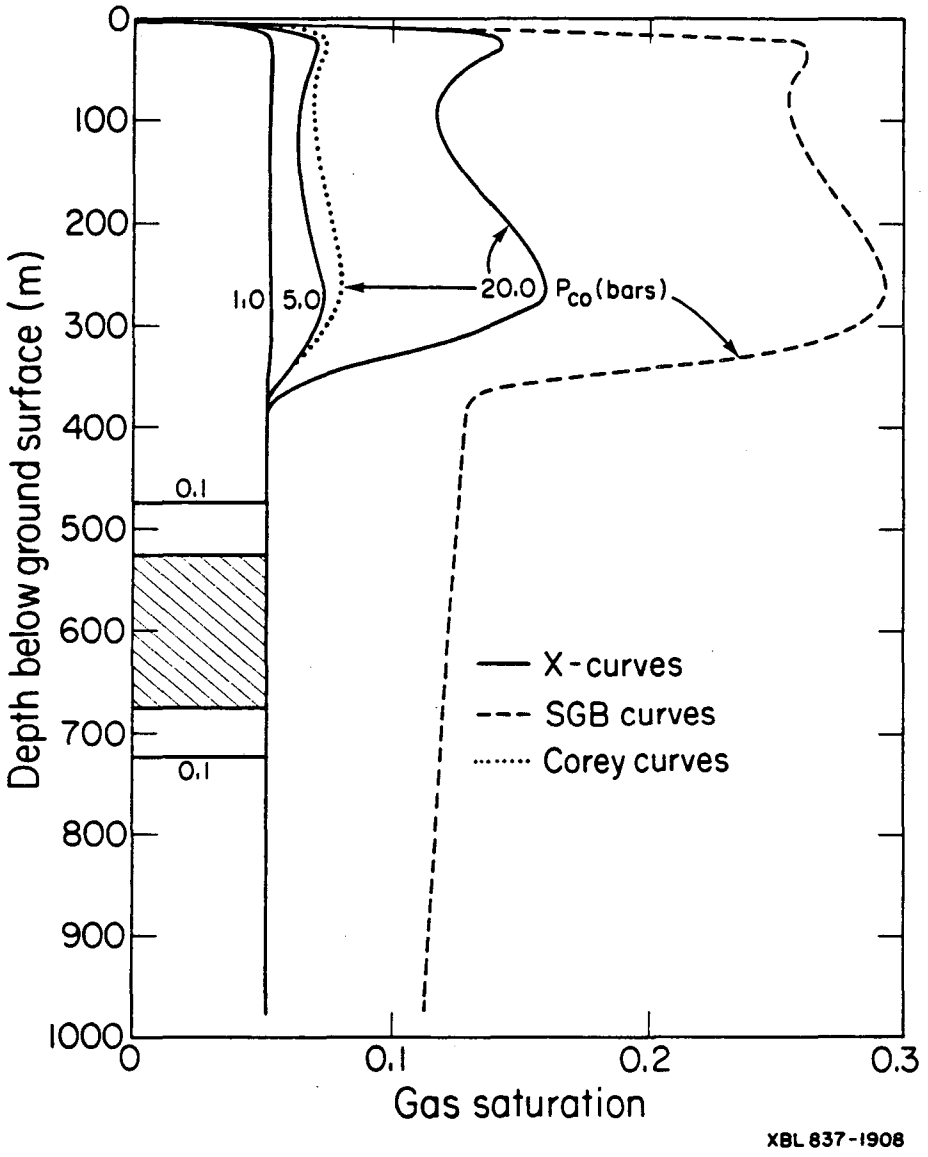

Figure 12. Vertical gas saturation profiles in gas-rich geothermal reservoirs.

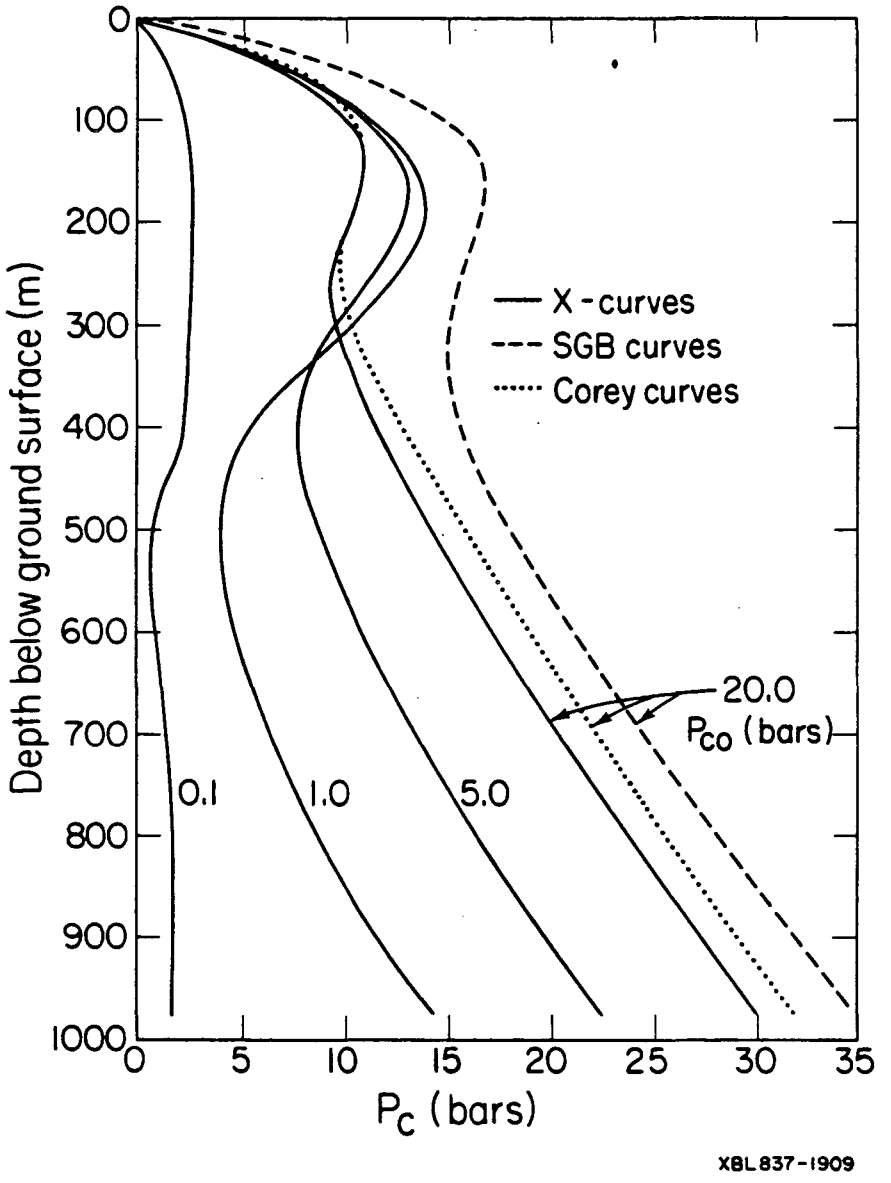

Figure 13. Vertical profiles of the partial pressure of CO_2 in a gas-rich geothermal reservoir.

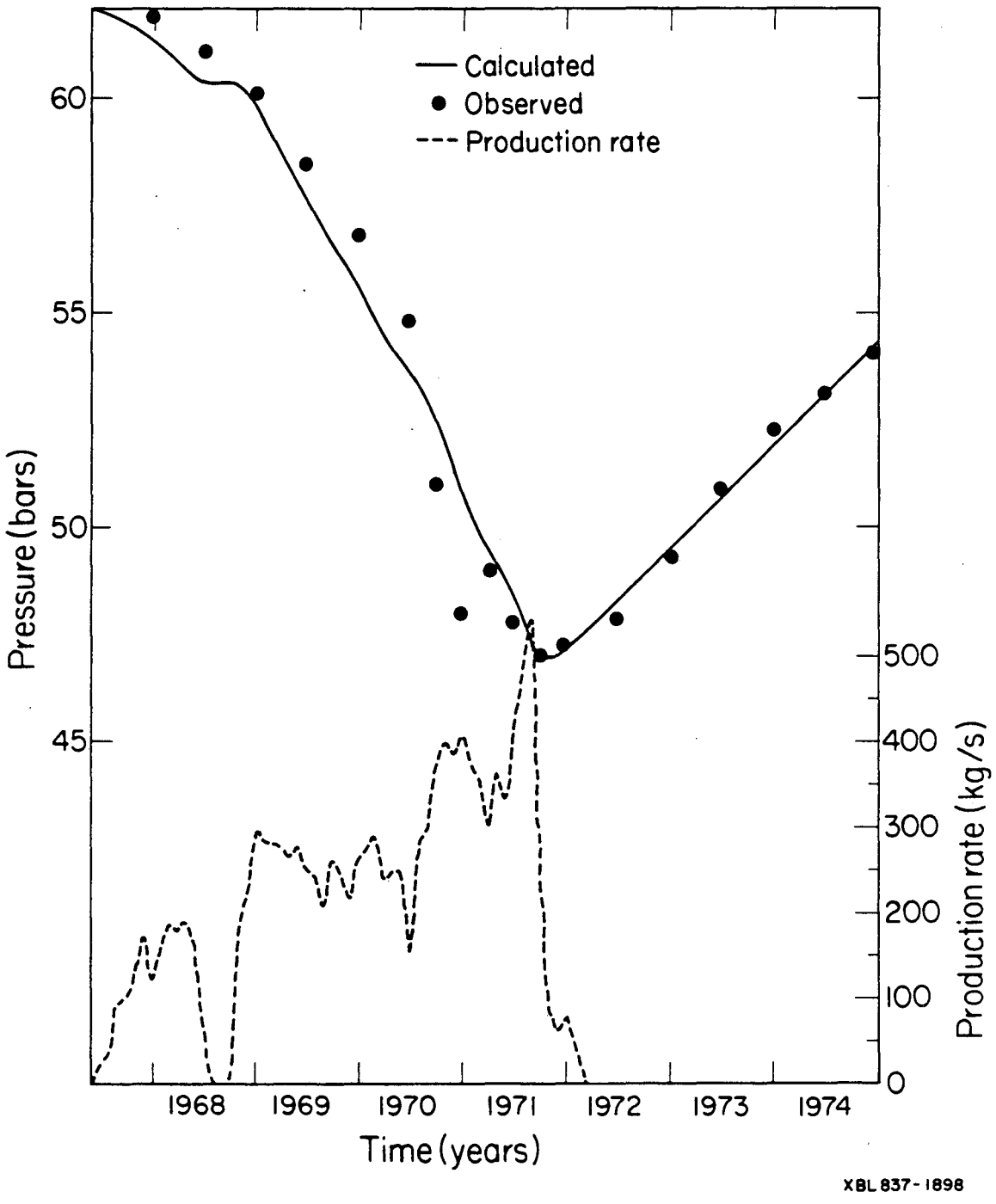

Figure 14. Comparison of the pressure decline in a simple lumped-parameter model of the Ohaaki reservoir with observed data.

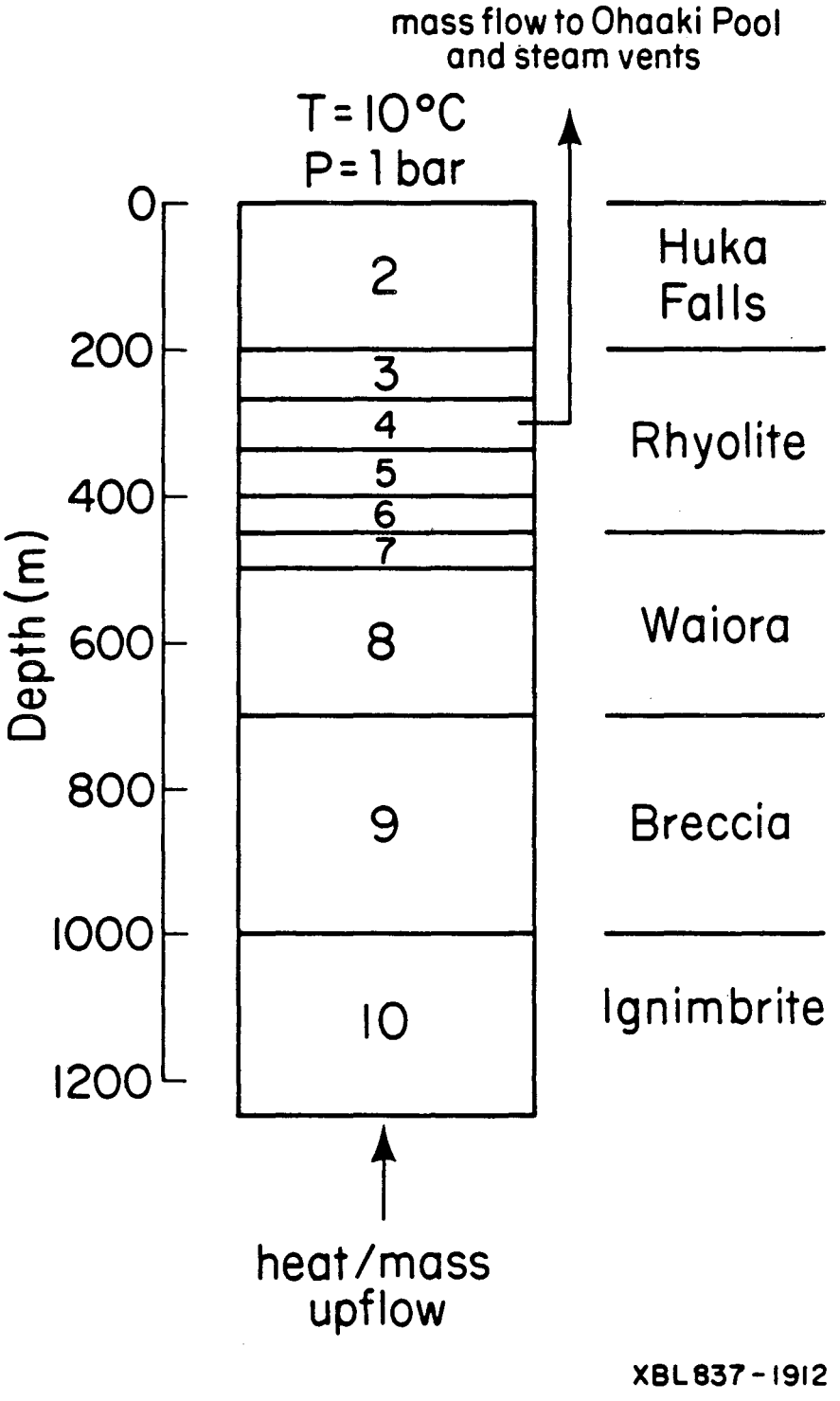

Figure 15. Vertical column model of the Ohaaki reservoir.

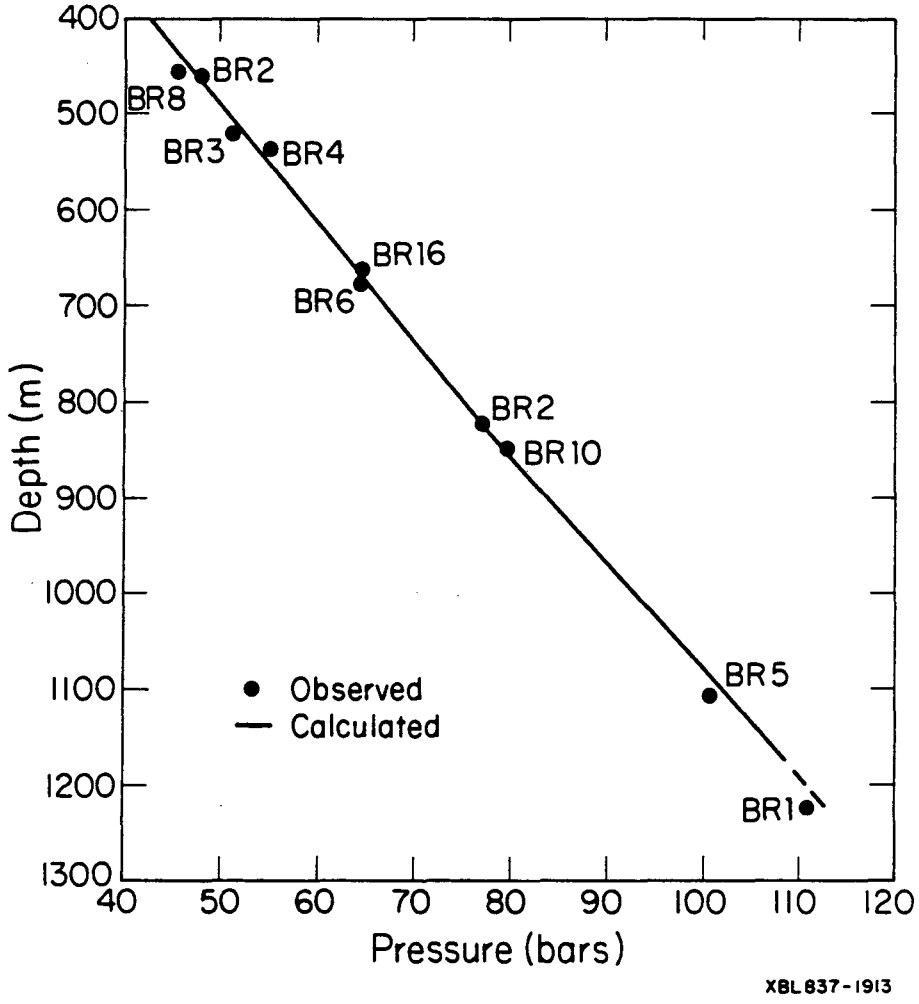

Figure 16. Vertical distribution of pressure in the natural-state model of Ohaaki.

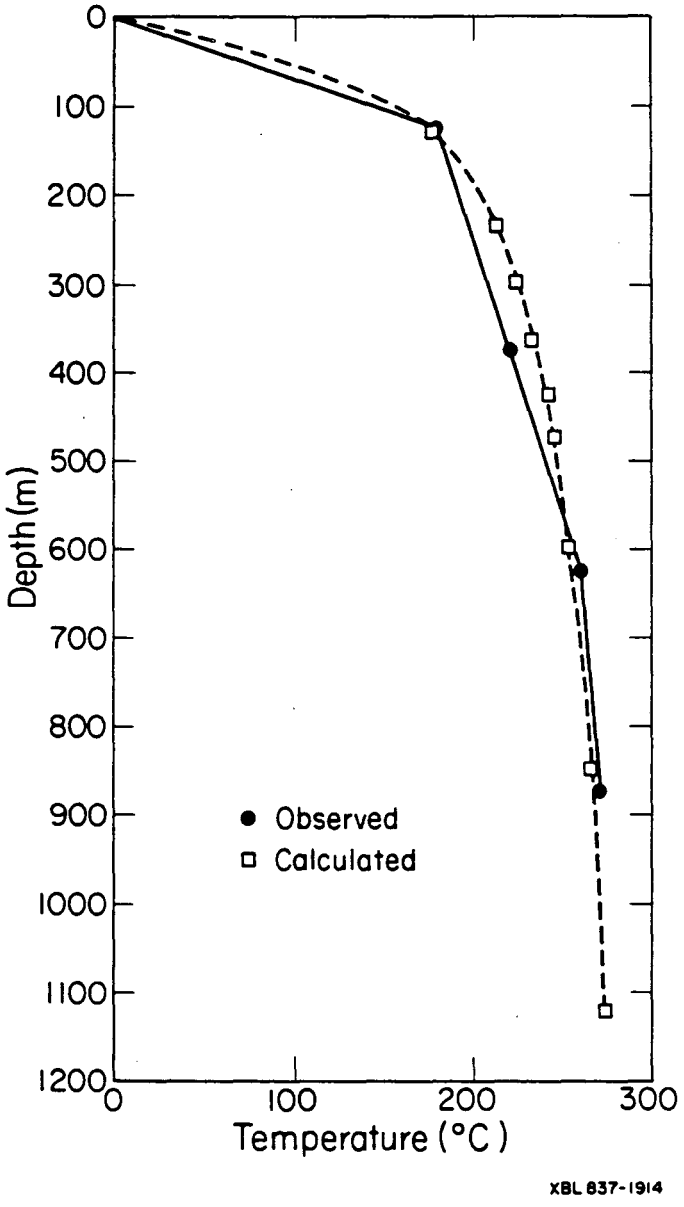

Figure 17. Vertical distribution of temperature in the natural-state model of Ohaaki.

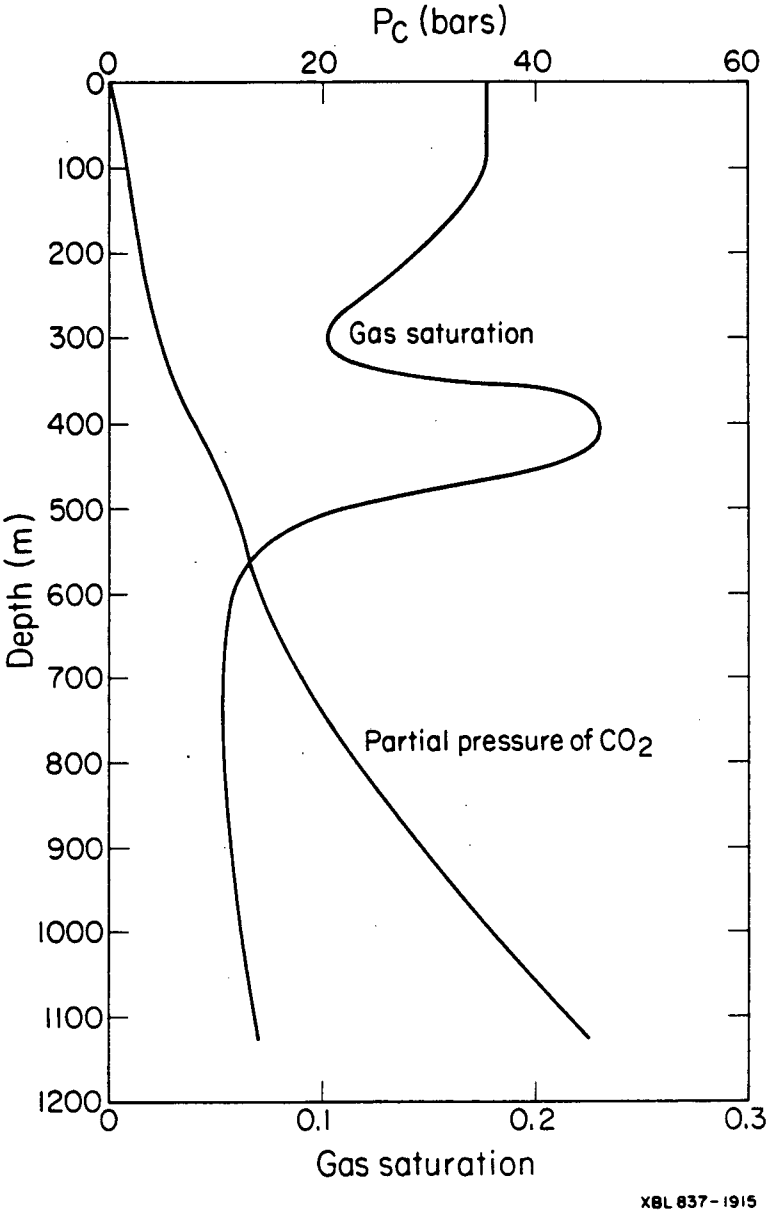

Figure 18. Vertical distribution of gas saturation and partial pressure of CO_2 in the natural-state model of Ohaaki.

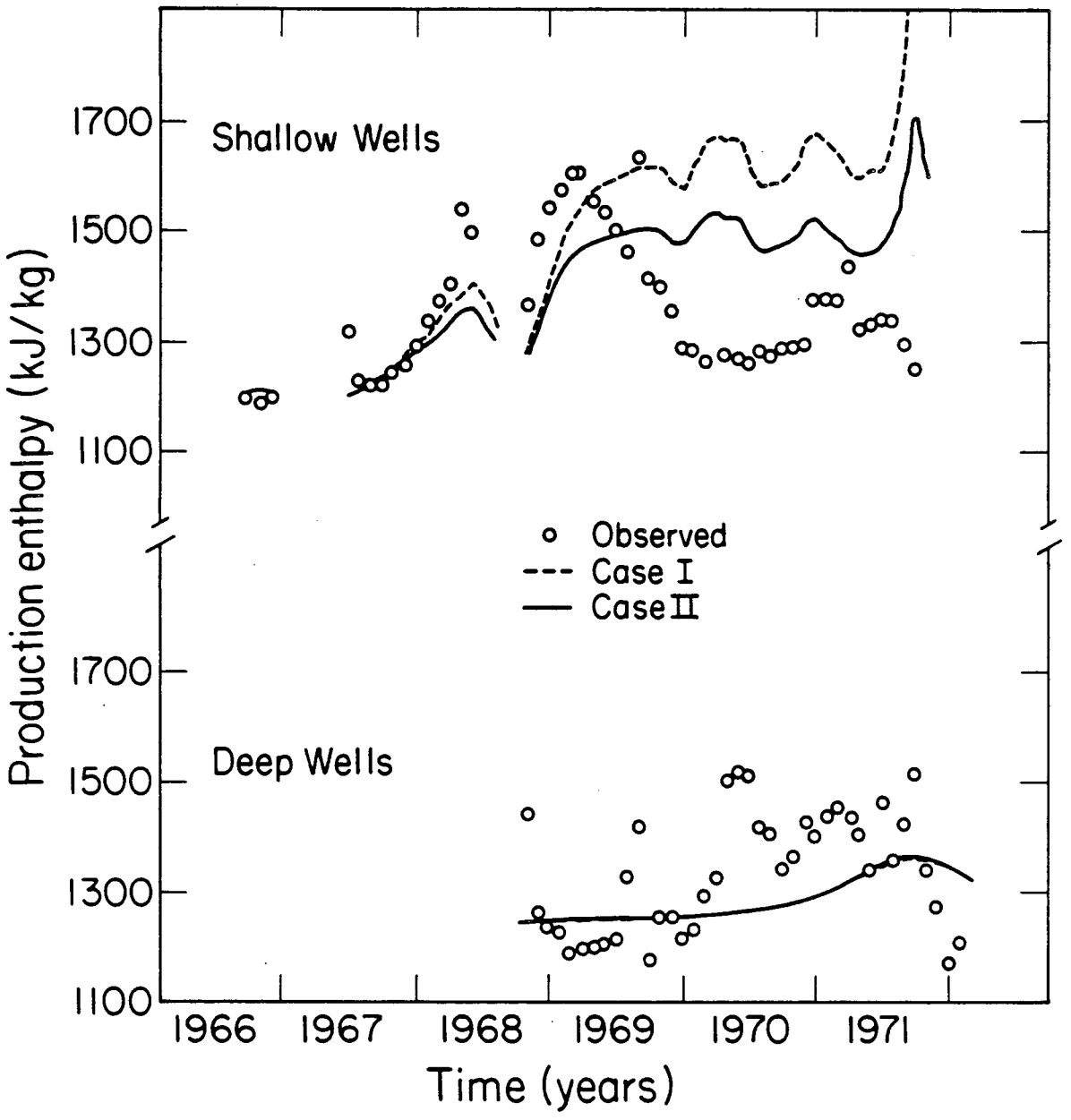

Figure 19. Production enthalpy for the vertical column Ohaaki model.

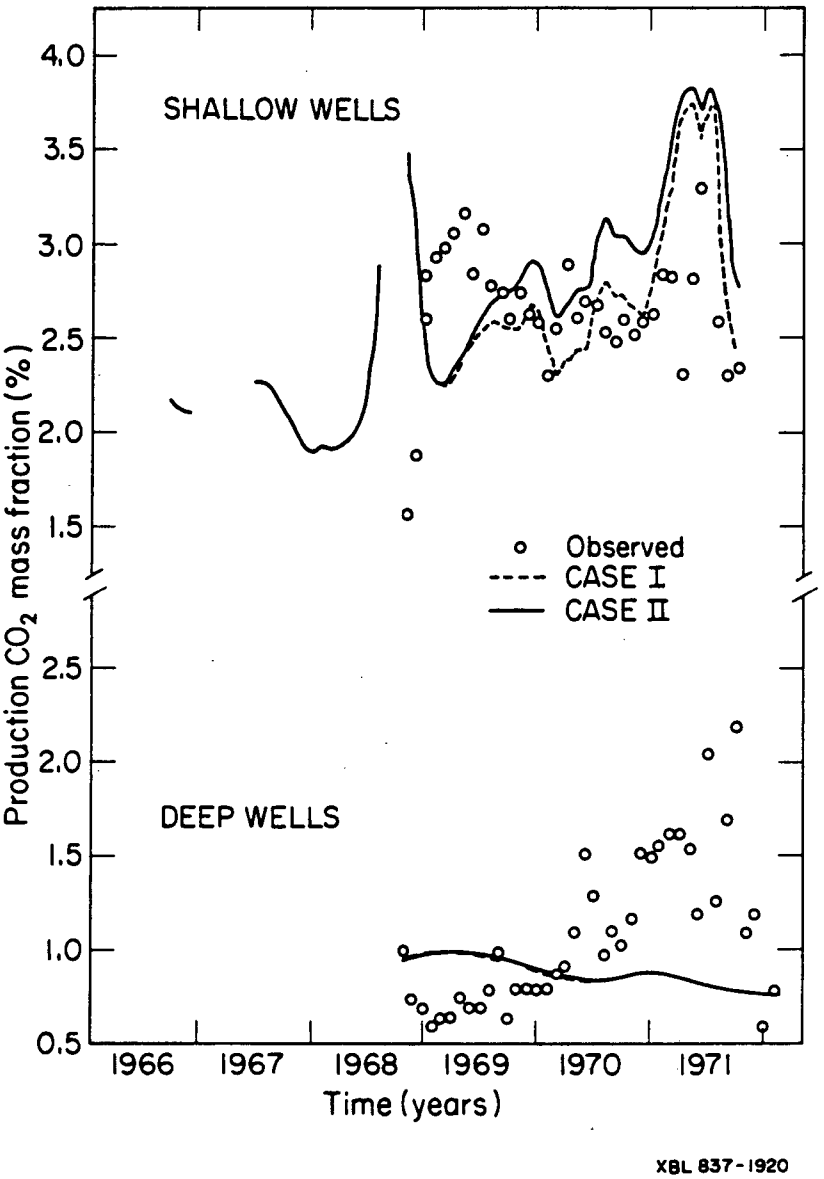

Figure 20. Production CO_2 mass fraction for the vertical column Ohaaki model.

TECHNICAL INFORMATION DEPARTMENT
LAWRENCE BERKELEY LABORATORY
UNIVERSITY OF CALIFORNIA
BERKELEY, CALIFORNIA 94720